AD-A078 785 PENNSYLVANIA STATE UNIV UNIVERSITY PARK APPLIED RESE--ETC F/G 20/11
VIBRATION OF A CLAMPED CIRCULAR PLATE DRIVEN BY A NONCENTRAL FO--ETC(U)
OCT 79 J C SNOWDON N00024-79-C-6043
UNCLASSIFIED ARL/PSU/TM-79-191 NL

| OF |
AD A078785

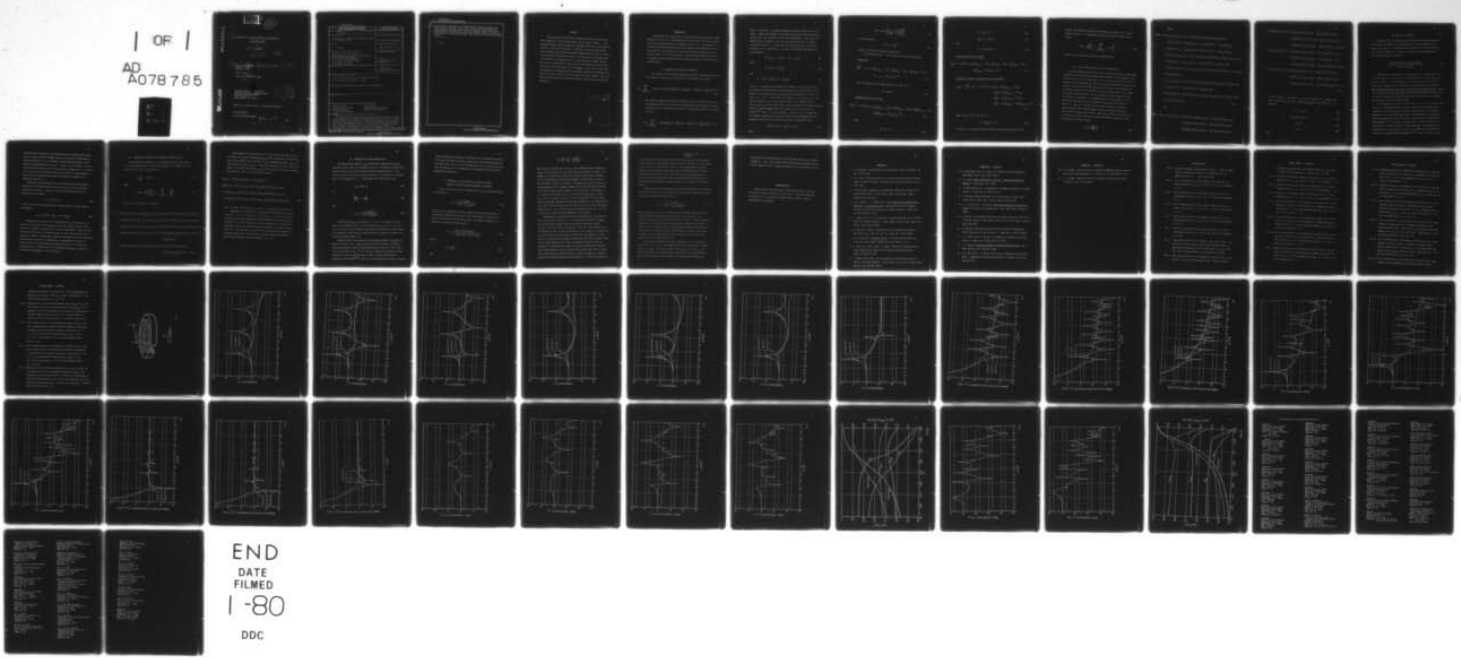

END
DATE FILMED
1-80
DDC

VIBRATION OF A CLAMPED CIRCULAR PLATE DRIVEN BY A NONCENTRAL FORCE.

by

J. C. Snowdon

31 Oct 79

57

Technical Memorandum
File No. 79-191
October 31, 1979

ARL/PSU/TM-79-191

Copy No. 46

Contract No. N00024-79-C-6043

The Pennsylvania State University
Institute for Science and Engineering
APPLIED RESEARCH LABORATORY
Post Office Box 30
State College, PA 16801

Approved for public release: distribution unlimited

NAVY DEPARTMENT

NAVAL SEA SYSTEMS COMMAND

UNCLASSIFIED

SECURITY CLASSIFICATION OF THIS PAGE (When Data Entered)

REPORT DOCUMENTATION PAGE		READ INSTRUCTIONS BEFORE COMPLETING FORM
1. REPORT NUMBER TM 79-191	2. GOVT ACCESSION NO.	3. RECIPIENT'S CATALOG NUMBER
4. TITLE (and Subtitle) Vibration of a Clamped Circular Plate Driven by a Noncentral Force		5. TYPE OF REPORT & PERIOD COVERED 6. PERFORMING ORG. REPORT NUMBER
7. AUTHOR(s) J. C. Snowdon		8. CONTRACT OR GRANT NUMBER(s) N00024-79-C-6043
9. PERFORMING ORGANIZATION NAME AND ADDRESS The Pennsylvania State University Applied Research Laboratory, P. O. Box 30, State College, PA 16801		10. PROGRAM ELEMENT, PROJECT, TASK AREA & WORK UNIT NUMBERS
11. CONTROLLING OFFICE NAME AND ADDRESS U. S. Naval Sea Systems Command Department of the Navy Washington, DC 20362		12. REPORT DATE October 31, 1979 13. NUMBER OF PAGES 57
14. MONITORING AGENCY NAME & ADDRESS(if different from Controlling Office)		15. SECURITY CLASS. (of this report) UNCLASSIFIED 15a. DECLASSIFICATION/DOWNGRADING SCHEDULE

16. DISTRIBUTION STATEMENT (of this Report)

Approved for public release; distribution unlimited.

(As per letter dated December 3, 1979.)

17. DISTRIBUTION STATEMENT (of the abstract entered in Block 20, if different from Report)

18. SUPPLEMENTARY NOTES

19. KEY WORDS (Continue on reverse side if necessary and identify by block number)

Transmissibility.
Clamped circular plate.
Internal damping.
Driving-point impedance.
Mass loading.
Dynamic vibration absorber.
Arbitrary driving point.

20. ABSTRACT (Continue on reverse side if necessary and identify by block number)

Expressions are stated for the transmissibility and for the driving-point impedance of an internally damped circular plate of radius a with a clamped boundary that is driven by a vibratory point force at an arbitrary distance μa from the plate center. Expressions are also stated for the plate transmissibility when the plate is loaded at the arbitrary driving point either by a lumped mass, by a dynamic vibration absorber--or, simultaneously, by a lumped mass and a dynamic absorber. In all cases,

DD FORM 1 JAN 73 1473 EDITION OF 1 NOV 65 IS OBSOLETE

UNCLASSIFIED

SECURITY CLASSIFICATION OF THIS PAGE (When Data Entered)

representative calculations of transmissibility are plotted versus the square root of frequency. These curves clearly show the dependence of transmissibility and impedance on the plate damping factor, the value of the parameter μ, and the extent of the mass loading. They also show the effectiveness of the dynamic absorber, which varies with the value assigned to μ.

mu

ABSTRACT

Expressions are stated for the transmissibility and for the driving-point impedance of an internally damped circular plate of radius a with a clamped boundary that is driven by a vibratory point force at an arbitrary distance μa from the plate center. Expressions are also stated for the plate transmissibility and driving-point impedance when the plate is loaded at the arbitrary driving point either by a lumped mass, by a dynamic vibration absorber--or, simultaneously by a lumped mass and a dynamic absorber. In all cases, representative calculations of transmissibility and impedance are plotted versus the square root of frequency. These curves clearly show the dependence of transmissibility and impedance on the plate damping factor, the value of the parameter μ, and the extent of the mass loading. They also show the effectiveness of the dynamic absorber, which varies with the value assigned to μ.

INTRODUCTION

The response of circular plates to noncentral forces has not been studied extensively in the past. The deformation of circular plates statically loaded off center has been discussed, for example, in Refs. 1-11. The response of a circular plate when transiently loaded off center has been addressed in Ref. 12. The response of circular plates to noncentral vibratory forces has been considered in Refs. 13-17, which represent a relatively small number of articles as compared to those concerned with the vibration response of centrally driven circular plates.

I. SOLUTION TO THE THIN-PLATE EQUATION

The solution to the thin-plate equation yields the following equation for the transverse deflection $\tilde{\xi}_k$ of the plate in its kth mode of vibration:

$$\tilde{\xi}_k = \sum_{k=0,1,2,\ldots} (A_k \cos k\theta + B_k \sin k\theta)[P_k^* J_k(n^* r) + Q_k^* Y_k(n^* r) + R_k^* I_k(n^* r) + S_k^* K_k(n^* r)]e^{j\omega t} , \tag{1}$$

and, when the origin of the polar coordinates is taken as the radial line passing through the point of excitation of the noncentral force (because a solution is required that is symmetrical with respect to this radial line) it is possible to write

$$\tilde{\xi}_k = \sum_{k=0,1,2,\ldots} \cos k\theta[P_k^* J_k(n^* r) + Q_k^* Y_k(n^* r) + R_k^* I_k(n^* r) + S_k^* K_k(n^* r)]e^{j\omega t} . \tag{2}$$

Here, t is time and ω is angular frequency, hereafter known simply as frequency. Symbols with superior tildes denote sinusoidally varying quantities, symbols with a star superscript denote complex quantities. The ordinary and modified Bessel functions of the first and second kinds have the complex argument $(n^* r)$ where r is the radius of the arbitrary point to which the noncentral force is applied (Fig. 1), and n^* is the plate wavenumber given by the equation

$$n^* = n\{[1 - (\nu^*)^2]/(1 - \nu^2)(1 + j\delta_{E\omega})\}^{1/4} \quad , \tag{3}$$

where

$$n^4 = \omega^2\rho(1 - \nu^2)/r_g^2 E_\omega \tag{4}$$

and

$$[1 - (\nu^*)^2] = (E_\omega^*/G_\omega^*)\ [1 - (E_\omega^*/4G_\omega^*)] \quad . \tag{5}$$

In Eq. (1), A_k and B_k are arbitrary real constants, and P_k^*, Q_k^*, R_k^*, and S_k^* are arbitrary complex constants, where Q_k^* and S_k^* are zero for a plate that is complete to the center because Y_k and K_k exhibit singularities as $(n^* r) \to 0$. In Eqs. (3) - (5), ρ is the density of the plate, a is its radius, r_g is the radius of gyration of its cross section, and ν^* is its complex Poisson's ratio; E_ω^* and G_ω^* are the complex Young's and shear moduli of the plate material. If their associated damping factors are equal, as can realistically be assumed,[18,19] then $\nu^* = \nu$, a real quantity. Further, if it is assumed that the frequency dependence of E_ω^* and G_ω^* and their associated damping factors is negligible (damping of the solid type or hysteretic damping[18]), then

$$(n^* a) = (na)/(1 + j\delta_E)^{1/4} = (p + jq) \quad , \tag{6}$$

where

$$p,q = \pm (na) \left[\frac{1}{2\sqrt{D_E}} \pm \frac{(1 + D_E)^{1/2}}{2\sqrt{2}\, D_E} \right] \quad ; \tag{7}$$

in this equation,

$$D_E = (1 + \delta_E^2)^{1/2} \quad , \tag{8}$$

where δ_E is the Young's modulus damping factor.

For the mode of order k it is possible to write the following:

Plate Slope

$$\frac{\partial \tilde{\xi}_k}{\partial r} = - n^* \cos k\theta \{P_k^*[J_{(k+1)} - T^* J_k] + Q_k^*[Y_{(k+1)} - T^* Y_k] - R_k^*[I_{(k+1)} + T^* I_k]$$

$$+ S_k^*[K_{(k+1)} - T^* K_k]\}_{(n^* r)} e^{j\omega t} \quad ; \tag{9}$$

where the argument of the Bessel functions is $(n^* r)$, and

$$T^* = k/(n^* r) \quad . \tag{10}$$

Bending Moment/Unit Arc Length

$$B_k(r) = - D^* (n^*)^2 \cos k\theta \{P_k^*[\phi_r^* J_{(k+1)} - \alpha^* J_k] + Q_k^*[\phi_r^* Y_{(k+1)} - \alpha^* Y_k] - R_k^*[\phi_r^* I_{(k+1)} - \varepsilon^* I_k]$$

$$+ S_R^*[\phi_r^* K_{(k+1)} + \varepsilon^* K_k]\}_{(n^* r)} e^{j\omega t} \quad , \tag{11}$$

where

$$\alpha^* = (1 - \Gamma^*) \quad , \tag{12}$$

$$\varepsilon^* = (1 + \Gamma^*) \quad , \tag{13}$$

$$\phi_r^* = (1 - \nu)/(n^* r) \quad , \tag{14}$$

and

$$\Gamma^* = k(k-1)\phi_r^*/(n\ r) \quad . \tag{15}$$

Shearing Force/Unit Arc Length

$$\tilde{F}_k(r) = - D^*(n^*)^3 \cos k\theta \{P_k^*[J_{(k+1)} - T^* J_k] + Q_k^*[Y_{(k+1)} - T^* Y_k] + R_k^*[I_{(k+1)} + T^* I_k] - S_k^*[K_{(k+1)} - T^* K_k]\}_{(n^* r)}\ e^{j\omega t} \quad . \tag{16}$$

Shearing Force/Unit Arc Length at the Plate Boundary

$$\begin{aligned}[\tilde{F}_k(r) - \frac{1}{r}\frac{\partial \tilde{B}_k}{\partial r}(r,\theta)] = - D^*(n^*)^3 \cos k\theta \{ & P_k^*[(1 + kT^*\phi_r^*)J_{(k+1)} - T^*\varepsilon^* J_k] \\ & + Q_k^*[(1 + kT^*\phi_r^*)Y_{(k+1)} - T^*\varepsilon^* Y_k] \\ & + R_k^*[(1 - kT^*\phi_r^*)I_{(k+1)} + T^*\alpha^* I_k] \\ & - S_k^*[(1 - kT^*\phi_r^*)K_{(k+1)} - T^*\alpha^* K_k]\}_{(n^* r)}\ e^{j\omega t} \quad ,\end{aligned} \tag{17}$$

where, in Eqs. (11), (16), and (17),

$$D^* = dE_\omega^* r_g^2/(1 - \nu^2) \tag{18}$$

in which d is the plate thickness and the radius of gyration $r_g = d/2\sqrt{3}$.

Finally, the impressed force/unit arc length at the radius $r = b = \mu a$ and angular location θ is conveniently represented by the following Fourier series:

$$\tilde{F}(\theta) = \frac{\tilde{F}_o}{2\pi b}\left[1 + 2\sum_{k=1,2,3,\ldots}^{\infty} \cos k\theta\right] , \qquad (19)$$

where $\tilde{F}_o$ is the concentrated (discrete) impressed force.

II. Force Transmissibility to the Plate Boundary

By considering the plate as two plates--a central plate plus a surrounding annular plate--that are joined together with continuity of displacement, slope, and bending moment at the same radius $r = b = \mu a$ as that to which the force is applied, and by considering the sum of the shearing force/unit arc length around the outer perimeter of the inner circular plate, and the shearing force/unit arc length around the inner perimeter of the outer annular plate, to be equal to the force specified by Eq. (19), by equating the displacement and slope of the plate to zero where it is clamped around its outer boundary, and by writing down the force that is transmitted to the outer plate boundary where $r = a$, then it is possible to write down six equations for the six complex constants for the entire plate (two for the inner circular plate and four for the outer annular plate). When these equations are solved for, it is possible to write down the following expression for the force transmissibility to the plate boundary:

$$T = \frac{1}{\mu}\left|\frac{(\text{NUM.})}{(\text{DEN.})}\right| , \qquad (20)$$

where

$$
\begin{aligned}
(\text{NUM.}) = \{&[(J_{1\mu}-T_\mu J_{o\mu})(\phi_\mu I_{1\mu}-\varepsilon I_{o\mu}) - (\phi_\mu J_{1\mu}-\alpha J_{o\mu})(I_{1\mu}+T_\mu I_{o\mu})][J_1 Y_{o\mu}(I_o K_1+K_o I_1) \\
&- J_1 K_{o\mu}(Y_o I_1+Y_1 I_o) + Y_1 K_{o\mu}(J_o I_1+J_1 I_o) + I_1 J_{o\mu}(Y_o K_1-Y_1 K_o) - I_1 Y_{o\mu}(J_o K_1-J_1 K_o) \\
&+ I_1 K_{o\mu}(J_o Y_1-J_1 Y_o) + I_1 K_o J_{o\mu}(Y_1-TY_o) + K_1 Y_{o\mu}(J_o I_1+J_1 I_o) - I_1 Y_o J_{o\mu}(K_1-TK_o)] \\
&+ [(Y_{1\mu}-T_\mu Y_{o\mu})(\phi_\mu I_{1\mu}-\varepsilon I_{o\mu})-(\phi_\mu Y_{1\mu}-\alpha Y_{o\mu})(I_{1\mu}+T_\mu I_{o\mu})][-J_1 I_o J_{o\mu}(K_1-TK_o)-J_1 K_o J_{o\mu}(I_1+TI_o) \\
&- I_1 K_o J_{o\mu}(J_1-TJ_o) - K_1 I_o J_{o\mu}(J_1-TJ_o) - J_o K_1 J_{o\mu}(I_1+TI_o) + J_o I_1 J_{o\mu}(K_1-TK_o)] \\
&+ [(\phi_\mu K_{1\mu}+\varepsilon K_{o\mu})(I_{1\mu}+T_\mu I_{o\mu})-(K_{1\mu}-T_\mu K_{o\mu})(\phi_\mu I_{1\mu}-\varepsilon I_{o\mu})]\{-J_{o\mu}J_1(Y_o I_1+Y_1 I_o)+J_{o\mu}Y_1(J_o I_1+J_1 I_o) \\
&+ J_{o\mu}I_1(J_o Y_1-J_1 Y_o)] \\
&+ [(Y_{1\mu}-T_\mu Y_{o\mu})(\phi_\mu J_{1\mu}-\alpha J_{o\mu})-(\phi_\mu Y_{1\mu}-\alpha Y_{o\mu})(J_{1\mu}-T_\mu J_{o\mu})][-J_1 K_o I_{o\mu}(I_1+TI_o)-J_1 I_o I_{o\mu}(K_1-TK_o) \\
&- K_1 J_o I_{o\mu}(I_1+TI_o) + I_1 I_{o\mu}(J_o K_1-J_1 K_o) - K_1 I_o I_{o\mu}(J_1-TJ_o)] \\
&+ [(K_{1\mu}-T_\mu K_{o\mu})(\phi_\mu J_{1\mu}-\alpha J_{o\mu})-(\phi_\mu K_{1\mu}+\varepsilon K_{o\mu})(J_{1\mu}-T_\mu J_{o\mu})][J_1 I_{o\mu}(Y_o I_1+Y_1 I_o)-Y_1 I_{o\mu}(J_o I_1+J_1 I_o) \\
&- I_1 I_{o\mu}(J_o Y_1-J_1 Y_o)]\}_{(n^* a)} \qquad (21)
\end{aligned}
$$

and

$$
\begin{aligned}
(\text{DEN.}) = \Delta_o^* = (Y_{1\mu}-T_\mu Y_{o\mu})(J_o I_1+J_1 I_o)\{&K_{o\mu}[(J_{1\mu}-T_\mu J_{o\mu})(\phi_\mu I_{1\mu}-\varepsilon I_{o\mu}) - (I_{1\mu}+T_\mu I_{o\mu})(\phi_\mu J_{1\mu}- J_{o\mu})] \\
&+ J_{o\mu}[(\phi_\mu K_{1\mu}+\varepsilon K_{o\mu})(I_{1\mu}+T_\mu I_{o\mu}) - (K_{1\mu}-T_\mu K_{o\mu})(\phi_\mu I_{1\mu}-\varepsilon I_{o\mu})] \\
&+ I_{o\mu}[(\phi_\mu K_{1\mu}+\varepsilon K_{o\mu})(J_{1\mu}-T_\mu J_{o\mu}) - (K_{1\mu}-T_\mu K_{o\mu})(\phi_\mu J_{1\mu}-\alpha J_{o\mu})]
\end{aligned}
$$

$$+ (K_{1\mu}-T_\mu K_{o\mu})(J_o I_1+J_1 I_o)\ \{Y_{o\mu}[(J_{1\mu}-T_\mu J_o)(\phi_\mu I_{1\mu}-\varepsilon I_{o\mu}) - (\phi_\mu J_{1\mu}-\alpha J_{o\mu})(I_{1\mu}+T_\mu I_{o\mu})]$$

$$+ J_{o\mu}[(\phi_\mu Y_{1\mu}-\alpha Y_{o\mu})(I_{1\mu}+T_\mu I_{o\mu}) - (\phi_\mu I_{1\mu}-\varepsilon I_{o\mu})(Y_{1\mu}-T_\mu Y_{o\mu})]$$

$$+ I_{o\mu}[(\phi_\mu Y_{1\mu}-\alpha Y_{o\mu})(J_{1\mu}-T_\mu J_{o\mu}) - (\phi_\mu J_{1\mu}-\alpha J_{o\mu})(Y_{1\mu}-T_\mu Y_{o\mu})]\}_{(n^*a)}$$

$$- (J_{1\mu}-T_\mu J_{o\mu})(J_o I_1+J_1 I_o)\ \{-Y_{o\mu}[(\phi_\mu K_{1\mu}+\varepsilon K_{o\mu})(I_{1\mu}+T_\mu I_{o\mu}) - (K_{1\mu}-T_\mu K_{o\mu})(\phi_\mu I_{1\mu}-\varepsilon I_{o\mu})]$$

$$+ K_{o\mu}[(\phi_\mu Y_{1\mu}-\alpha Y_{o\mu})(I_{1\mu}+T_\mu I_{o\mu}) - (Y_{1\mu}-T_\mu Y_{o\mu})(\phi_\mu I_1-\varepsilon I_{o\mu})]$$

$$+ I_{o\mu}[(\phi_\mu Y_{1\mu}-\alpha Y_{o\mu})(K_{1\mu}-T_\mu K_{o\mu}) - (Y_{1\mu}-T_\mu Y_{o\mu})(\phi_\mu K_{1\mu}+\varepsilon K_{o\mu})]\}_{(n^*a)}$$

$$+ (I_{1\mu}+T_\mu I_{o\mu})(J_o I_1+J_1 I_o)\ \{Y_{o\mu}[(K_{1\mu}-T_\mu K_{o\mu})(\phi_\mu J_{1\mu}-\alpha J_{o\mu}) - (\phi_\mu K_{1\mu}+\varepsilon K_{o\mu})(J_{1\mu}-T_\mu J_{o\mu})]$$

$$- K_{o\mu}[(Y_{1\mu}-T_\mu Y_{o\mu})(\phi_\mu J_{1\mu}-\alpha J_{o\mu}) - (\phi_\mu Y_{1\mu}-\alpha Y_{o\mu})(J_{1\mu}-T_\mu J_{o\mu})]$$

$$- J_{o\mu}[(\phi_\mu Y_{1\mu}-\alpha Y_{o\mu})(K_{1\mu}-T_\mu K_{o\mu}) - (Y_{1\mu}-T_\mu Y_{o\mu})(\phi_\mu K_{1\mu}+\varepsilon K_{o\mu})]\}_{(n^*a)} \qquad (22)$$

In these equations, such terms as $J_{1\mu}$, $I_{o\mu}$, K_1, and Y_o, etc., represent the Bessel functions $J_{(k+1)}(\mu n^* a)$, $I_k(\mu n^* a)$, $K_{(k+1)}(n^* a)$, and $Y_k(n^* a)$, etc.; in addition,

$$T = T^* = k/(n^* a) \quad , \qquad (23)$$

$$T_\mu = T_\mu^* = k/(\mu n^* a) \quad , \qquad (24)$$

$$\alpha = \alpha^* \quad , \qquad (25)$$

$$\varepsilon = \varepsilon^* \quad , \qquad (26)$$

and

$$\phi_\mu = \phi_\mu^* = (1 - \nu)/(\mu n^* a) \quad . \tag{27}$$

A much more concise expression for transmissibility can be obtained by the principle of reciprocity as the magnitude of the displacement of the plate at the radius r = μa divided by the displacement of the plate boundary (r = a) when the boundary is vibrated sinusoidally. The simple expression that can be obtained is as follows:

$$T = \left| \frac{J_1(n^* a) I_o(\mu n^* a) + I_1(n^* a) J_o(\mu n^* a)}{(J_1 I_o + I_1 J_o)(n^* a)} \right| \quad . \tag{28}$$

Representative calculations of transmissibility T are plotted in Figs. 2-6 for values of μ = 0.2, 0.5, 0.75, 0.2548 and 0.379; ν = 1/3, and $\delta_E = \delta_G$ = 0.01, 0.1, and 1.0. In these figures, the horizontal axis is (na)--a real dimensionless quantity that is proportional to the square root of frequency. Only the symmetrical plate modes (k = 0) contribute to transmissibility. Whereas it is true that all other plate modes are excited by the noncentral force, the net upward and downward transmitted forces that they generate at the clamped plate boundary cancel one another exactly.

The transmissibility curves of Figs. 2-4 (μ = 0.2, 0.5, 0.75) exhibit peak values at the symmetrical plate resonances--the extent of the amplification depending on the plate damping, the largest value of which is considered as a hypothetical case since the dynamic Young's and shear moduli associated with such high damping would not be constant, as assumed here, but would increase with frequency.[18] In all cases, transmissibility is equal to unity at low frequencies, as should be expected. Also as expected, the appearance of the transmissibility curves when μ = 0.2 (Fig. 2) resembles those obtained previously for a centrally driven clamped plate.[20] In Fig. 5, where μ = 0.379,

the second plate resonance is not excited because the impressed force then lies on a nodal circle of the mode; rather, in its place a broad region of attenuation where $T < 1.0$ is introduced between bounds that differ in frequency by an approximate factor of 4.5. Again, in Fig. 6, when $\mu = 0.2548$, the third plate resonance is not excited because the impressed force coincides with a nodal circle of the mode; rather, in its place is a broad region of attenuation that extends between bounds that differ in frequency by an approximate factor of 2.7.

Should the plate be driven by two vibratory forces of like magnitude and phase at two arbitrary points, radii $\mu_1 a$ and $\mu_2 a$, then the resultant force transmissibility is obtained by writing the transmissibility for a single force in the form

$$T = \left|(a + jb)_{\mu}\right| \quad ; \tag{29}$$

so that, for the dual-force excitation, transmissibility is given simply by the equation

$$T_{1,2} = \tfrac{1}{2} \left|[(a + jb)_{\mu_1} + (a + jb)_{\mu_2}]\right| \quad . \tag{30}$$

Representative calculations of transmissibility $T_{1,2}$ for dual-force excitation with the point forces applied at the pairs of radii 0.2944a, 0.490a, and 0.2547a, 0.583a, are shown in Figs. 7 and 8, respectively. These locations were chosen judiciously to eliminate evidence of the second and third plate resonances. Rather, in their place, regions of attenuation have been introduced between bounds that differ in frequency by the approximate factors of 5.0 (Fig. 7) and 4.0--or, discounting the single peak where $na = 6.3$ (Fig. 8) by a factor of 10.5. In these, and in all subsequent calculations, values of k in the range of <u>at least</u> 1-15 were considered.

III. DRIVING-POINT IMPEDANCE AT ARBITRARY LOCATION ON PLATE

The driving-point impedance Z_μ of the plate at the arbitrary radius $r = \mu a$, when normalized by division by the impedance of a lumped mass equal to the plate mass M_p, can be written as

$$\frac{Z_\mu}{j\omega M_p} = -\,1/(\text{DEN.}) \quad , \tag{31}$$

where

$$(\text{DEN.}) = \left(\frac{n^* a}{2\mu}\right)\left\{\frac{\Xi_o^*}{\Delta_o^*} + 2\sum_{k=1,2,3,\ldots}^{\infty}\frac{\Xi_k^*}{\Delta_k^*}\right\} \quad . \tag{32}$$

In Eq. (32), Ξ_k^* is given by the equation

$$\begin{aligned}
\Xi_k^* = \{ & [(Y_{1\mu}-\tau_\mu Y_\mu)(\phi_\mu J_{1\mu}-\alpha J_\mu)-(\phi_\mu Y_{1\mu}-\alpha Y_\mu)(J_{1\mu}-\tau_\mu J_\mu)][I_\mu K_\mu(JI_1+IJ_1)+I_\mu^2(JK_1-KJ_1)-J_\mu I_\mu(IK_1+KI_1)] \\
& + [(\phi_\mu K_{1\mu}+\varepsilon K_\mu)(I_{1\mu}+\tau_\mu I_\mu)-(K_{1\mu}-\tau_\mu K_\mu)(\phi_\mu I_{1\mu}-\varepsilon I_\mu)][-J_\mu^2(YI_1+IY_1)+J_\mu I_\mu(JY_1-YJ_1)+J_\mu Y_\mu(IJ_1+JI_1)] \\
& + [(\phi_\mu Y_{1\mu}-\alpha Y_\mu)(I_{1\mu}+\tau_\mu I_\mu)-(Y_{1\mu}-\tau_\mu Y_\mu)(\phi_\mu I_{1\mu}-\varepsilon I_\mu)][J_\mu^2(KI_1+IK_1)-J_\mu K_\mu(JI_1+IJ_1)-J_\mu I_\mu(JK_1-KJ_1)] \\
& + [(\phi_\mu J_{1\mu}-\alpha J_\mu)(I_{1\mu}+\tau_\mu I_\mu)-(J_{1\mu}-\tau_\mu J_\mu)(\phi_\mu I_{1\mu}-\varepsilon I_\mu)][-J_\mu Y_\mu(KI_1+IK_1)+J_\mu K_\mu(YI_1+IY_1)-K_\mu I_\mu(JY_1-YJ_1) \\
& \qquad + Y_\mu I_\mu(JK_1-KJ_1)] \\
& + [(\phi_\mu J_{1\mu}-\alpha J_\mu)(K_{1\mu}-\tau_\mu K_\mu)-(J_{1\mu}-\tau_\mu J_\mu)(\phi_\mu K_{1\mu}+\varepsilon K_\mu)][J_\mu I_\mu(YI_1+IY_1)-Y_\mu I_\mu(JI_1+IJ_1) \\
& \qquad - I_\mu^2(JY_1-YJ_1)]\}_{(n^* a)} \cos k\theta \quad . \qquad (33)
\end{aligned}$$

The parameter Δ_o^* is given by Eq. (22), Ξ_o^* is given by Eq. (33) in which such terms as $Y_{1\mu}$ and Y_μ representing $Y_{(k+1)}(\mu n^* a)$ and $Y_k(\mu n^* a)$ are replaced by $Y_1(\mu n^* a)$ and $Y_o(\mu n^* a)$, and such terms as J, I_1 representing $J_k(n^* a)$, $I_{(k+1)}(n^* a)$ are replaced by $J_o(n^* a)$, $I_1(n^* a)$. Again, Δ_k^* is given by Eq. (22) in which such terms as $Y_{1\mu}$ and $Y_{o\mu}$ now become $Y_{(k+1)}(\mu n^* a)$ and $Y_k(\mu n^* a)$ so that, for example, the first term of Eq. (22) should read as follows:

$$
\begin{aligned}
&(Y_{(k+1)\mu} - T_\mu Y_{k\mu})(n^* a)(J_k I_{(k+1)} + I_k J_{(k+1)})(n^* a) \times \\
&\{K_{k\mu}[(J_{(k+1)\mu} - T_\mu J_{k\mu})(\phi_\mu I_{(k+1)\mu} - \varepsilon I_{k\mu}) - (I_{(k+1)\mu} + T_\mu I_{k\mu})(\phi_\mu J_{(k+1)\mu} - \alpha J_{k\mu})] \\
&+ J_{k\mu}[(\phi_\mu K_{(k+1)\mu} + \varepsilon K_{k\mu})(I_{(k+1)\mu} + T_\mu I_{k\mu}) - (K_{(k+1)\mu} - T_\mu K_{k\mu})(\phi_\mu I_{(k+1)\mu} - \varepsilon I_{k\mu})] \\
&+ I_{k\mu}[(\phi_\mu K_{(k+1)\mu} + \varepsilon K_{k\mu})(J_{(k+1)\mu} - T_\mu J_{k\mu}) - (K_{(k+1)\mu} - T_\mu K_{k\mu})(\phi_\mu J_{(k+1)\mu} - \alpha J_{k\mu})]\}(n^* a) \quad . \qquad (34)
\end{aligned}
$$

Here, as before, the terms T_μ, ϕ_μ, α, and ε are given by Eqs. (24)-(27).

Representative calculations of $|Z_\mu / j\omega M_p|$ are plotted in Figs. 9-11 for values of $\mu = 0.2$, 0.5, and 0.75, $\nu = 1/3$, and $\delta_E = \delta_G = 0.01$, 0.1, and 1.0. Evidence is now seen of every mode of plate vibration--both symmetrical and nonsymmetrical. At low frequencies, the plate impedance is very large and springlike--so that the normalized impedance diminishes inversely in proportion to ω^2. The impedance alternately exhibits minima (plate resonances) and maxima (plate antiresonances) that lie almost symmetrically about the heavily damped impedance curve for which $\delta_E = \delta_G = 1.0$.

IV. VIBRATION OF THE MASS-LOADED PLATE

The driving-point impedance $Z_{\mu m}$ and the force transmissibility $T_{\mu m}$ of the plate of Fig. 1 when it is loaded by a mass M at the point of application of the noncentral force follow directly from the foregoing results. Thus, since there must be continuity of motion between M and the plate, it follows that, if the loading mass is γ times greater than the plate mass M_p,

$$Z_{\mu m} = j\omega M + Z_{\mu} \tag{35}$$

or

$$\frac{Z_{\mu m}}{j\omega M_p} = \gamma + \frac{Z_{\mu}}{j\omega M_p} \tag{36}$$

and

$$T_{\mu m} = T_{\mu} \left| \frac{(Z_{\mu}/j\omega M_p)}{\gamma + (Z_{\mu}/j\omega M_p)} \right| \quad . \tag{37}$$

Calculations of $T_{\mu m}$ for a value of $\gamma = 1.0$, $\nu = 1/3$, and $\mu = 0.2$, 0.5 and 0.75, are plotted in Figs. 12-14 for values of $\delta_E = \delta_G = 0.01$, 0.1, and 1.0. Now, because the nonsymmetric plate modes are excited due to the presence of the noncentral mass loading, essentially twice the number of resonances are excited than before (Figs. 2-4).

Companion plots of the normalized driving-point impedance $|Z_{\mu m}/j\omega M_p|$ are presented in Figs. 15-17. Again, essentially twice the number of resonances (minima of impedance, maxima of transmissibility) are observed. Notice how, in all these figures (Figs. 12-17), the plate resonances are shifted to lower frequencies by the mass loading (such a shift is always observed when a structure is mass loaded[18,20]); and how, at low frequencies, the plate impedance

remains springlike in character. Also notice that the normalized impedances of the plate at higher frequencies exhibit only limited fluctuations about the value unity; this is to say, the impressed force is primarily presented with the impedance of the loading mass--the impedance of the plate being negligible by comparison.

V. VIBRATION OF A PLATE DRIVEN OFF CENTER AT A POINT TO WHICH A DYNAMIC VIBRATION ABSORBER IS ATTACHED

In this situation, the force transmissibility T_a to the plate boundary can be written as

$$T_a = T_\mu \left| \frac{(Z_\mu / j\omega M_p)}{[\Psi^* + (Z_\mu / j\omega M_p)]} \right| , \tag{38}$$

where T_μ and $(Z_\mu / j\omega M_p)$ are the force transmissibility and the normalized driving-point impedance of the plate at the driving point located at the arbitrary distance μa from the plate center. The complex parameter Ψ^* is given by the relatively simple equation

$$\Psi^* = \frac{\gamma_a [1 + 2j(\omega_m/\omega_a)\Omega_m \delta_R]}{[1 - (\omega_m/\omega_a)^2 \Omega_m^2 + 2j(\omega_m/\omega_a)\Omega_m \delta_R]} , \tag{39}$$

where

$$\gamma_a = M_a / M_p \tag{40}$$

and

$$\Omega_m = \frac{\omega}{\omega_{11}} = \frac{\omega}{\omega_m} = \frac{(na)^2}{(3.1962)^2} \quad . \tag{41}$$

Here, M_a is the absorber mass and ω_{11} is the fundamental plate frequency to which, in this instance, but not necessarily, the absorber is tuned. [For example, if the absorber is tuned to the second or third plate resonance, Eq. (41) would remain relevant but the number (3.1962) would be replaced by the numbers (6.3064) or (9.4395).] The quantities $(\omega_m/\omega_a)^{-1}$ and δ_R are design parameters of the dynamic absorber and they must be chosen carefully if the full potential of the absorber is to be realized. For example, if μ is small and if the mass ratio $\gamma_a = 0.1$ or 0.25, then $(\omega_a/\omega_m) = 0.698$, $\delta_R = 0.408$, or $(\omega_a/\omega_m) = 0.465$, $\delta_R = 0.549$, respectively.[21] These values yield near-optimum conditions for which the two maxima in the transmissibility curve take essentially equal values a little to each side of the fundamental plate resonance. They assume that the plate damping factors $\delta_E = \delta_G = 0.01$, a value that is adopted for the remainder of this section.

Representative calculations of the transmissibility T_a are plotted in Figs. 18 and 19 for a value of $\mu = 0.2$ and for pairs of values of (ω_a/ω_m) and δ_R that differ slightly from those previously specified; namely, $(\omega_a/\omega_m) = 0.698$, $\delta_R = 0.462$, and $(\omega_a/\omega_m) = 0.493$, $\delta_R = 0.546$, respectively. The absorbers of Figs. 18 and 19 are seen to be most effective in suppressing the plate resonance to which they are tuned; they also suppress, to some extent, the higher plate resonances--particularly the heavier absorber, which has the larger damping ratio. Thus, at frequencies above the absorber resonance, the absorber mass becomes an almost stationary point from which the absorber dashpot is able to restrain the resonant plate motion, and the force transmissibility across the plate, at higher frequencies. Companion curves for the dynamic absorbers (mass ratios $\gamma_a = 0.1$ and 0.25) located at

the radial distance 0.75a from the plate center, for which the plate impedance is approximately 30 times greater than at the radial distance 0.2a, are plotted in Figs. 20 and 21, respectively. Because of the larger value of the plate impedance, to attain equal peak heights near the fundamental plate resonance proved more difficult than usual. Other values of the optimum tuning and damping ratios and the companion values of maximum transmissibility at the fundamental plate resonance are plotted in Fig. 22 as a function of the parameter μ.

Should the plate be mass loaded at the point of attachment of the dynamic absorber, then the force transmissibility T_{ma} to the plate boundary can readily be stated from inspection of Eq. (38) as

$$T_{ma} = T_{\mu m} \left| \frac{(Z_{\mu m}/j\omega M_p)}{[\Psi^* + (Z_{\mu m}/j\omega M_p)]} \right| , \qquad (42)$$

where $(Z_{\mu m}/j\omega M_p)$ and $T_{\mu m}$ are the normalized driving-point impedance and force transmissibility of the mass-loaded plate [Eqs. (36) and (37)] at the arbitrary driving point distance μa from the plate center. In this situation, the parameter γ (factor by which the loading mass exceeds the plate mass) is equated to 1.0; the same values of (ω_a/ω_m) and δ_R (parameters that appear in Ψ^*) as before are initially chosen, and thenchanges are made in their values to equalize the two transmissibility maxima because, to begin with, these maxima will only be approximately equal.

Representative calculations of T_{ma} are plotted in Figs. 23 and 24 for values of $\gamma = 1.0$, $\gamma_a = 0.1$; and, again, values of $\mu = 0.2$ and 0.75. Optimum values of $(\omega_a/\omega_m) = 0.356$, $\delta_R = 0.119$, and of $(\omega_a/\omega_m) = 0.761$, $\delta_R = 0.139$, respectively, are seen to provide equal suppression of the transmissibility peaks at the fundamental plate resonance; now, however, the loading mass

causes the force transmissibility to fall off quite rapidly at all higher frequencies. Again, other values of the optimum tuning and damping ratios, and the companion values of maximum transmissibility are plotted in Fig. 25.

ACKNOWLEDGMENTS

Especial thanks are due to Adah A. Wolfe for her help in obtaining the results presented graphically in this report. The investigation was sponsored by the U. S. Naval Sea Systems Command, and this support is acknowledged with gratitude.

REFERENCES

1. J. H. Michelle, "The Flexure of a Circular Plate," Proc. London Math. Soc. 34, 223-228 (1902).

2. R. J. Roark, "Stresses Produced in a Circular Plate by Eccentric Loading and by a Transverse Couple," The University of Wisconsin Bulletin No. 74, 1-41 (1932).

3. A. M. Sen Gupta, "Bending of a Cylindrically Aeolotropic Circular Plate with Eccentric Load," J. Appl. Mechs., Trans. Am. Soc. Mech. Engrs., Series E, 19, 9-12 (1952).

4. M. A. Goldberg, T. L. Hoffa, and J. Gorga, Analysis of an Annular Plate Subjected to a Concentrated Load, Polytechnic Institute of Brooklyn, Department of Aerospace Engineering and Applied Mechanics, PIBAL Rept. No. 68-2 (February, 1962).

5. J. Dundurs and T.-M. Lee, "Flexure by a Concentrated Force of the Infinite Plate on a Circular Support," J. Appl. Mechs., Trans. Am. Soc. Mech. Engrs., Series E, 30, 225-231 (1963).

6. R. Amon and J. Dundurs, "Supported Plate with Supported Edge Beam," J. Eng. Mechs. Divn., Proc. Am. Soc. Civ. Engrs. 94, 731-742 (1968).

7. S. G. Lekhnitskii, Anisotropic Plates, Translated from the Russian by S. W. Tsai and T. Cheron, (Gordon and Breach, 1968), p. 376.

8. R. Amon, O. E. Widera, and R. G. Ahrens, "Problem of the Annular Plate, Simply Supported and Loaded with an Eccentric Concentrated Force," AIAA J. 8, 961-963 (1970).

9. Y. Takeuti and N. Noda, "On a Measurement of Various Shaped Plates by Optical Interference Method," J. Appl. Mechs., Trans. Am. Soc. Mech. Engrs., Series E, 37, 1182-1186 (1970).

REFERENCES -- CONTINUED

10. B. Moustakakis and J. F. Carney, III, "Annular Plate with Supporting Edge Beams," AIAA J. 10, 529-531 (1972).

11. R. Szilard, Theory and Analysis of Plates: Classical and Numerical Methods, (Prentice-Hall, Inc., 1974).

12. R. Ramakrishnan and V. X. Kunukkasseril, "Asymmetric Response of Circular Plates," J. Sound Vib. 34, 489-504 (1974).

13. H. Reissman, "Forced Vibrations of a Circular Plate," J. Appl. Mech., Trans. Am. Soc. Mech. Engrs., Series E, 26, 526-527 (1959).

14. A. J. McLeod and R. E. D. Bishop, The Forced Vibration of Circular Flat Plates, Mech. Engr. Sci, Monograph No. 1, Inst. Mech. Engrs. (London), (1965).

15. A. Kalnins, "On Fundamental Solutions and Green's Functions in the Theory of Elastic Plates," J. Appl. Mech., Trans, Am. Soc. Mech. Engrs., Series E, 33, 31-38 (1966).

16. G. Anderson, "On the Determination of Finite Integral Transforms for Forced Vibrations of Circular Plates," J. Sound Vib. 9, 126-144 (1969).

17. D. S. Potter and C. D. Leedham, "Antisymmetric Vibrations of a Circular Plate," J. Acoust. Soc. Am. 49, 1521-1526 (1971).

18. J. C. Snowdon, Vibration and Shock in Damped Mechanical Systems (John Wiley and Sons, Inc., New York, 1968).

19. R. L. Kerlin and J. C. Snowdon, "Driving-Point Impedances of Cantilever Beams -- Comparison of Measurement and Theory," J. Acoust. Soc. Am. 47, 220-228 (1970).

REFERENCES -- CONTINUED

20. J. C. Snowdon, "Forced Vibration of Internally Damped Circular and Annular Plates with Clamped Boundaries," J. Acoust. Soc. Am. 50, 846-858 (1971).

21. J. C. Snowdon, "Mechanical Four-Pole Parameters and their Application," J. Sound Vib. 15, 307-323 (1971).

FIGURE LEGENDS

Fig. 1 An internally damped circular plate of radius a that is clamped around its boundary and driven by a vibratory force at an arbitrary distance μa from the plate center.

Fig. 2 Force transmissibility to the boundary of the plate of Fig. 1; plate damping factors $\delta_E = \delta_G = 0.01$, 0.1, and 1.0; the parameter $\mu = 0.2$.

Fig. 3 Force transmissibility to the boundary of the plate of Fig. 1; plate damping factors $\delta_E = \delta_G = 0.01$, 0.1, and 1.0; the parameter $\mu = 0.5$.

Fig. 4 Force transmissibility to the boundary of the plate of Fig. 1; plate damping factors $\delta_E = \delta_G = 0.01$, 0.1, and 1.0; the parameter $\mu = 0.75$.

Fig. 5 Force transmissibility to the boundary of the plate of Fig. 1; plate damping factors $\delta_E = \delta_G = 0.01$, 0.1, and 1.0; the parameter $\mu = 0.379$.

Fig. 6 Force transmissibility to the boundary of the plate of Fig. 1; plate damping factors $\delta_E = \delta_G = 0.01$, 0.1, and 1.0; the parameter $\mu = 0.2548$.

Fig. 7 Force transmissibility to the boundary of the plate of Fig. 1 when the plate is driven simultaneously by dual vibratory forces of equal phase and magnitude; plate damping factors $\delta_E = \delta_G = 0.01$, 0.1, and 1.0; the parameters $\mu_1 = 0.2944a$ and $\mu_2 = 0.490a$.

Fig. 8 Force transmissibility to the boundary of the plate of Fig. 1 when the plate is driven simultaneously by dual vibratory forces of

FIGURE LEGENDS -- CONTINUED

equal phase and magnitude; plate damping factors $\delta_E = \delta_G = 0.01$, 0.1, and 1.0; the parameters $\mu_1 = 0.2547a$ and $\mu_2 = 0.583a$.

Fig. 9 Normalized driving-point impedance of the plate of Fig. 1; plate damping factors $\delta_E = \delta_G = 0.01$, 0.1, and 1.0; the parameter $\mu = 0.2$.

Fig. 10 Normalized driving-point impedance of the plate of Fig. 1; plate damping factors $\delta_E = \delta_G = 0.01$, 0.1, and 1.0; the parameter $\mu = 0.5$.

Fig. 11 Normalized driving-point impedance of the plate of Fig. 1; plate damping factors $\delta_E = \delta_G = 0.01$, 0.1, and 1.0; the parameter $\mu = 0.75$.

Fig. 12 Force transmissibility to the boundary of the plate of Fig. 1 when the plate is loaded at the driving point by a lumped mass equal to the plate mass ($\gamma = 1.0$); plate damping factors $\delta_E = \delta_G = 0.01$, 0.1, and 1.0; the parameter $\mu = 0.2$.

Fig. 13 Force transmissibility to the boundary of the plate of Fig. 1 when the plate is loaded at the driving point by a lumped mass equal to the plate mass ($\gamma = 1.0$); plate damping factors $\delta_E = \delta_G = 0.01$, 0.1, and 1.0; the parameter $\mu = 0.5$.

Fig. 14 Force transmissibility to the boundary of the plate of Fig. 1 when the plate is loaded at the driving point by a lumped mass equal to the plate mass ($\gamma = 1.0$); plate damping factors $\delta_E = \delta_G = 0.01$, 0.1, and 1.0; the parameter $\mu = 0.75$.

Fig. 15 Normalized driving-point impedance of the plate of Fig. 1 when the plate is loaded at the driving point by a lumped mass equal to the plate mass ($\gamma = 1.0$); plate damping factors $\delta_E = \delta_G = 0.01$, 0.1, and 1.0; the parameter $\mu = 0.2$.

FIGURE LEGENDS -- CONTINUED

Fig. 16 Normalized driving-point impedance of the plate of Fig. 1 when the plate is loaded at the driving point by a lumped mass equal to the plate mass ($\gamma = 1.0$); plate damping factors $\delta_E = \delta_G = 0.01$, 0.1, and 1.0; the parameter $\mu = 0.5$.

Fig. 17 Normalized driving-point impedance of the plate of Fig. 1 when the plate is loaded at the driving point by a lumped mass equal to the plate mass ($\gamma = 1.0$); plate damping factors $\delta_E = \delta_G = 0.01$, 0.1, and 1.0; the parameter $\mu = 0.75$.

Fig. 18 Force transmissibility to the boundary of the plate of Fig. 1 when a dynamic vibration absorber is attached to the plate at the arbitrary driving point. Mass ratio $\gamma_a = 0.1$; optimum tuning and damping ratios $(\omega_a/\omega_m) = 0.698$, $\delta_R = 0.462$; the parameter $\mu = 0.2$; the plate damping factors $\delta_E = \delta_G = 0.01$.

Fig. 19 Force transmissibility to the boundary of the plate of Fig. 1 when a dynamic vibration absorber is attached to the plate at the arbitrary driving point. Mass ratio $\gamma_a = 0.25$; optimum tuning and damping ratios $(\omega_a/\omega_m) = 0.493$, $\delta_R = 0.546$. The parameter $\mu = 0.2$; the plate damping factors $\delta_E = \delta_G = 0.01$.

Fig. 20 Force transmissibility to the boundary of the plate of Fig. 1 when a dynamic vibration absorber is attached to the plate at the arbitrary driving point. Mass ratio $\gamma_a = 0.1$; optimum tuning and damping ratios $(\omega_a/\omega_m) = 0.980$, $\delta_R = 0.089$. The parameter $\mu = 0.75$; the plate damping factors $\delta_E = \delta_G = 0.01$.

Fig. 21 Force transmissibility to the boundary of the plate of Fig. 1 when a dynamic vibration absorber is attached to the plate at the

FIGURE LEGENDS -- CONTINUED

arbitrary driving point. Mass ratio $\gamma_a = 0.25$; optimum tuning and damping ratios $(\omega_a/\omega_m) = 0.950$, $\delta_R = 0.182$. The parameter $\mu = 0.75$; the plate damping factors $\delta_E = \delta_G = 0.01$.

Fig. 22 Optimum values of the tuning and damping ratios (ω_a/ω_m) and δ_R, and the companion values of the maximum transmissibility T_{max} at the fundamental plate resonance plotted as a function of the parameter μ; the plate damping factors $\delta_E = \delta_G = 0.01$. For the dashed- and solid-line curves, the mass ratio $\gamma_a = 0.1$ and 0.25, respectively.

Fig. 23 Force transmissibility to the boundary of the plate of Fig. 1 when both a lumped mass and a dynamic vibration absorber are attached to the plate at the arbitrary driving point. Mass ratios $\gamma = 1.0$, $\gamma_a = 0.1$; optimum tuning and damping ratios $(\omega_a/\omega_m) = 0.356$, $\delta_R = 0.119$. The parameter $\mu = 0.2$; the plate damping factors $\delta_E = \delta_G = 0.01$.

Fig. 24 Force transmissibility to the boundary of the plate of Fig. 1 when both a lumped mass and a dynamic vibration absorber are attached to the plate at the arbitrary driving point. Mass ratios $\gamma = 1.0$, $\gamma_a = 0.1$; optimum tuning and damping ratios $(\omega_a/\omega_m) = 0.761$, $\delta_R = 0.139$. The parameter $\mu = 0.75$; the plate damping factors $\delta_E = \delta_G = 0.01$.

Fig. 25 Optimum values of the tuning and damping ratios (ω_a/ω_m) and δ_R, and the companion values of the maximum transmissibility T_{max} at the fundamental plate resonance plotted as a function of the parameter μ; the plate damping factors $\delta_E = \delta_G = 0.01$. For the dashed- and solid-line curves, the mass ratio $\gamma_a = 0.1$ and 0.25, respectively. For both curves, the mass ratio $\gamma = 1.0$.

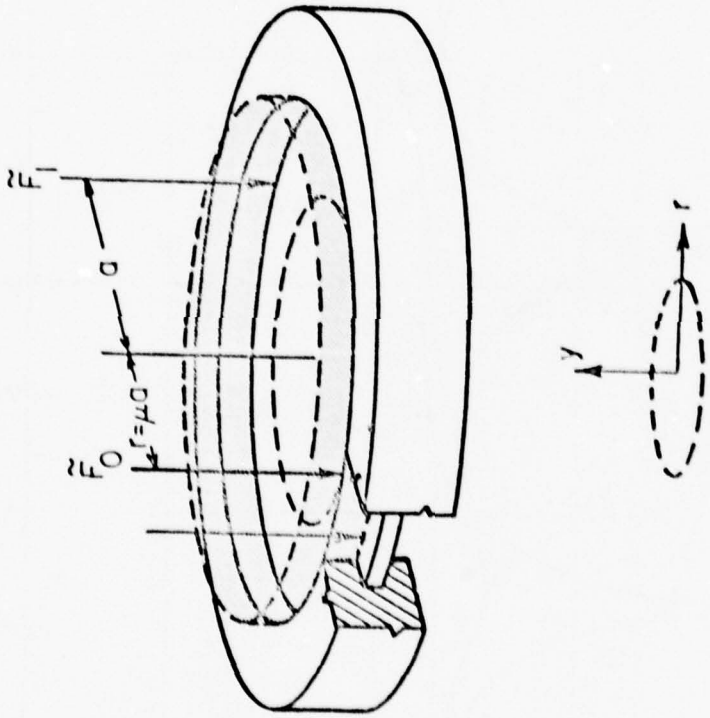

FIG. 1

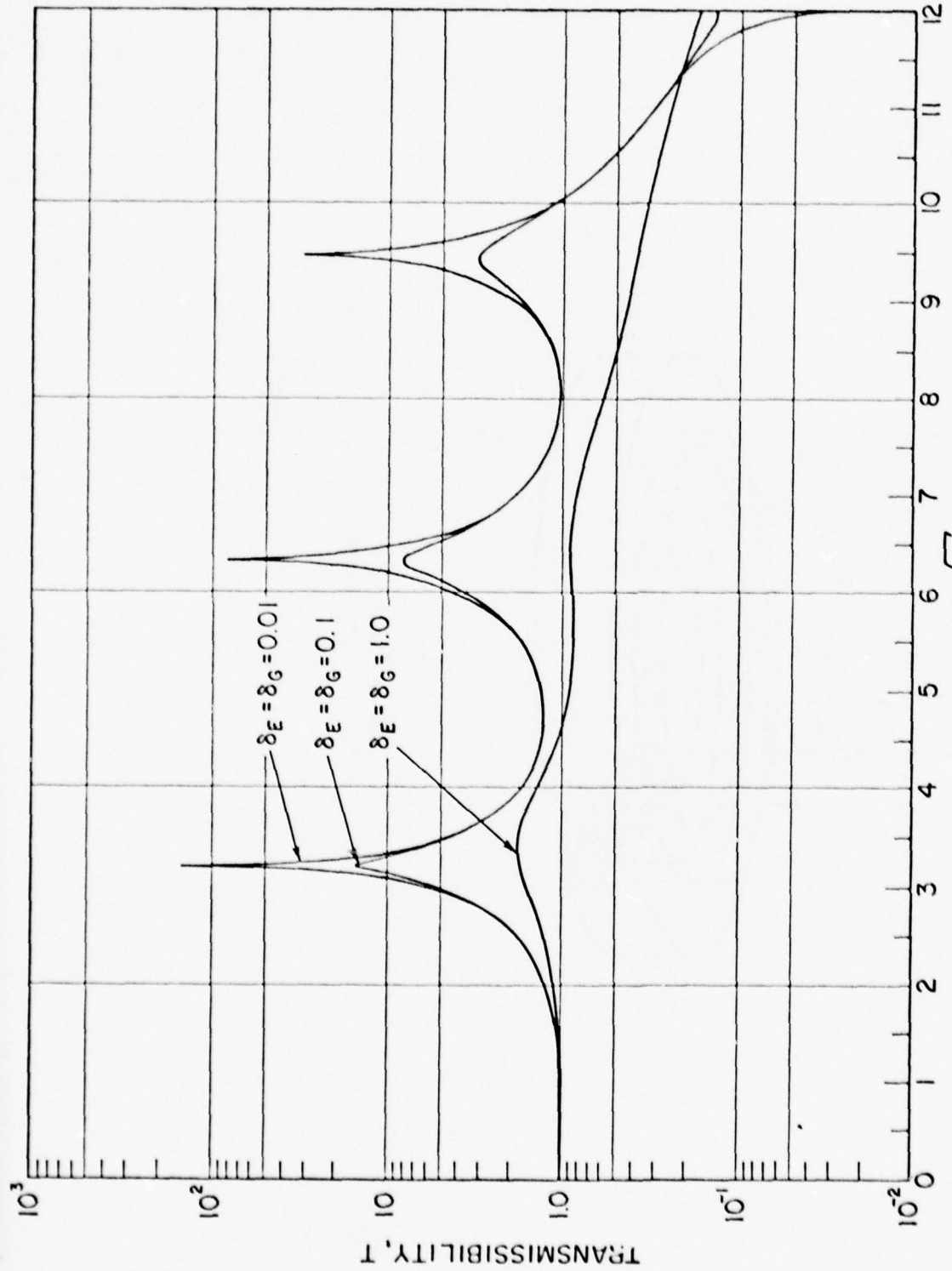
TRANSMISSIBILITY, T
10^{3}
10^{2}
10
1.0
10^{-1}
10^{-2}
0
1
2
3
4
5
6
7
8
9
10
11
12
$n a \alpha \sqrt{\omega}$
$\delta_E = \delta_G = 0.01$
$\delta_E = \delta_G = 0.1$
$\delta_E = \delta_G = 1.0$

FIG. 2

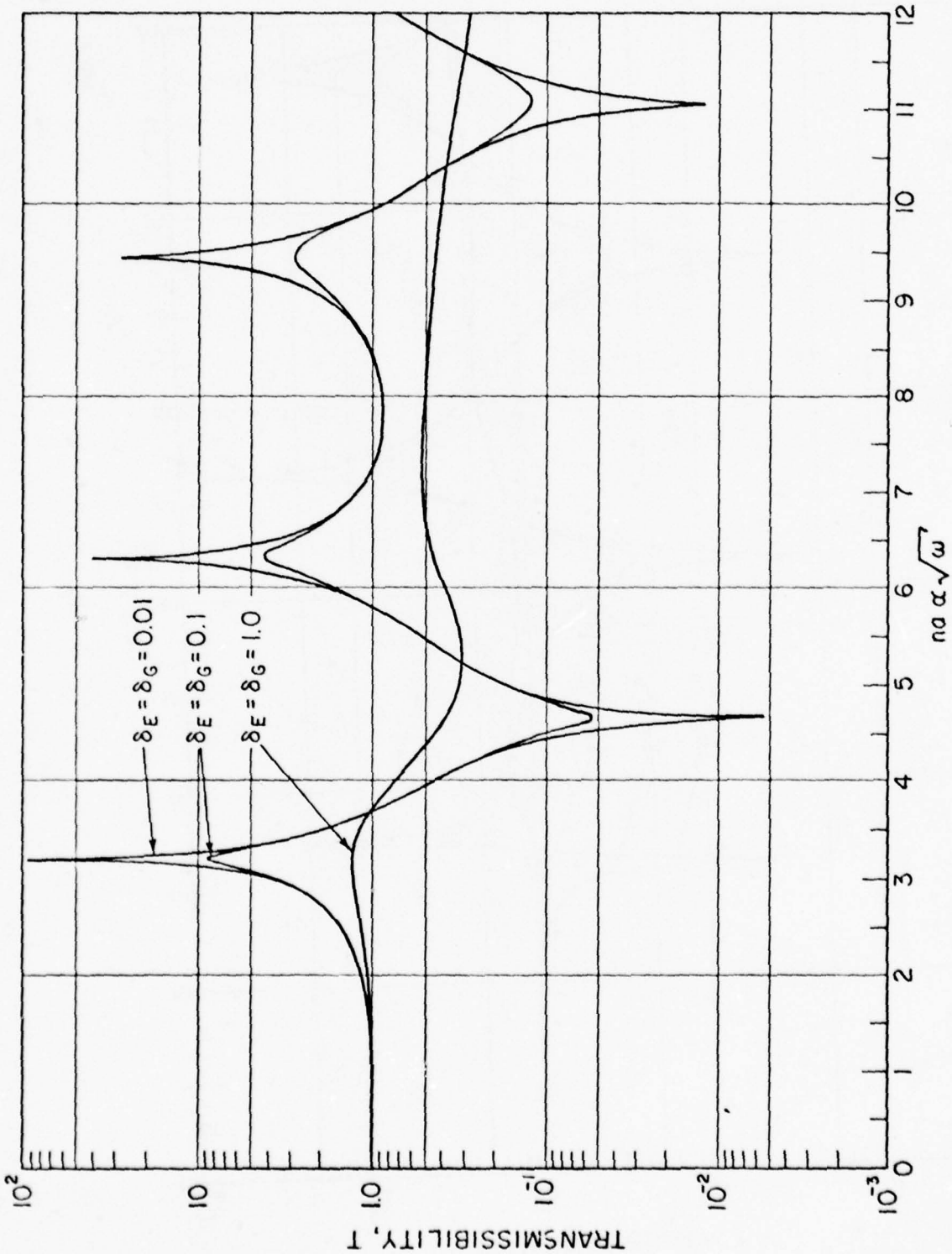
TRANSMISSIBILITY, T
10^{2}
10
1.0
10^{-1}
10^{-2}
10^{-3}
0
1
2
3
4
5
6
7
8
9
10
11
12
$\delta_E = \delta_G = 0.01$
$\delta_E = \delta_G = 0.1$
$\delta_E = \delta_G = 1.0$
$na\alpha\sqrt{\omega}$

FIG. 3

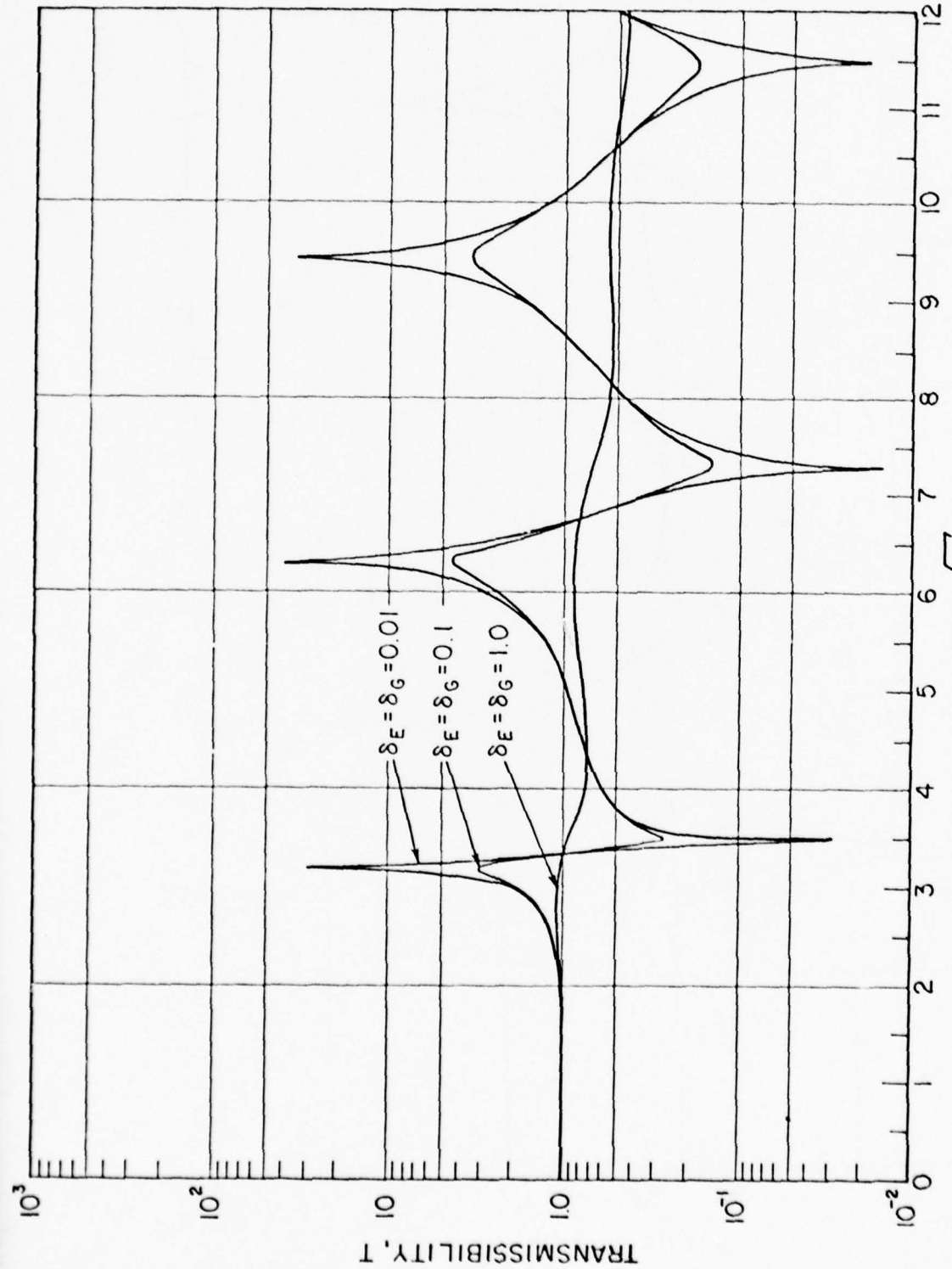
TRANSMISSIBILITY, T
10^{3}
10^{2}
10
1.0
10^{-1}
10^{-2}
0
1
2
3
4
5
6
7
8
9
10
11
12
$\delta_E=\delta_G=0.01$
$\delta_E=\delta_G=0.1$
$\delta_E=\delta_G=1.0$
$na\alpha\sqrt{\omega}$

FIG. 4

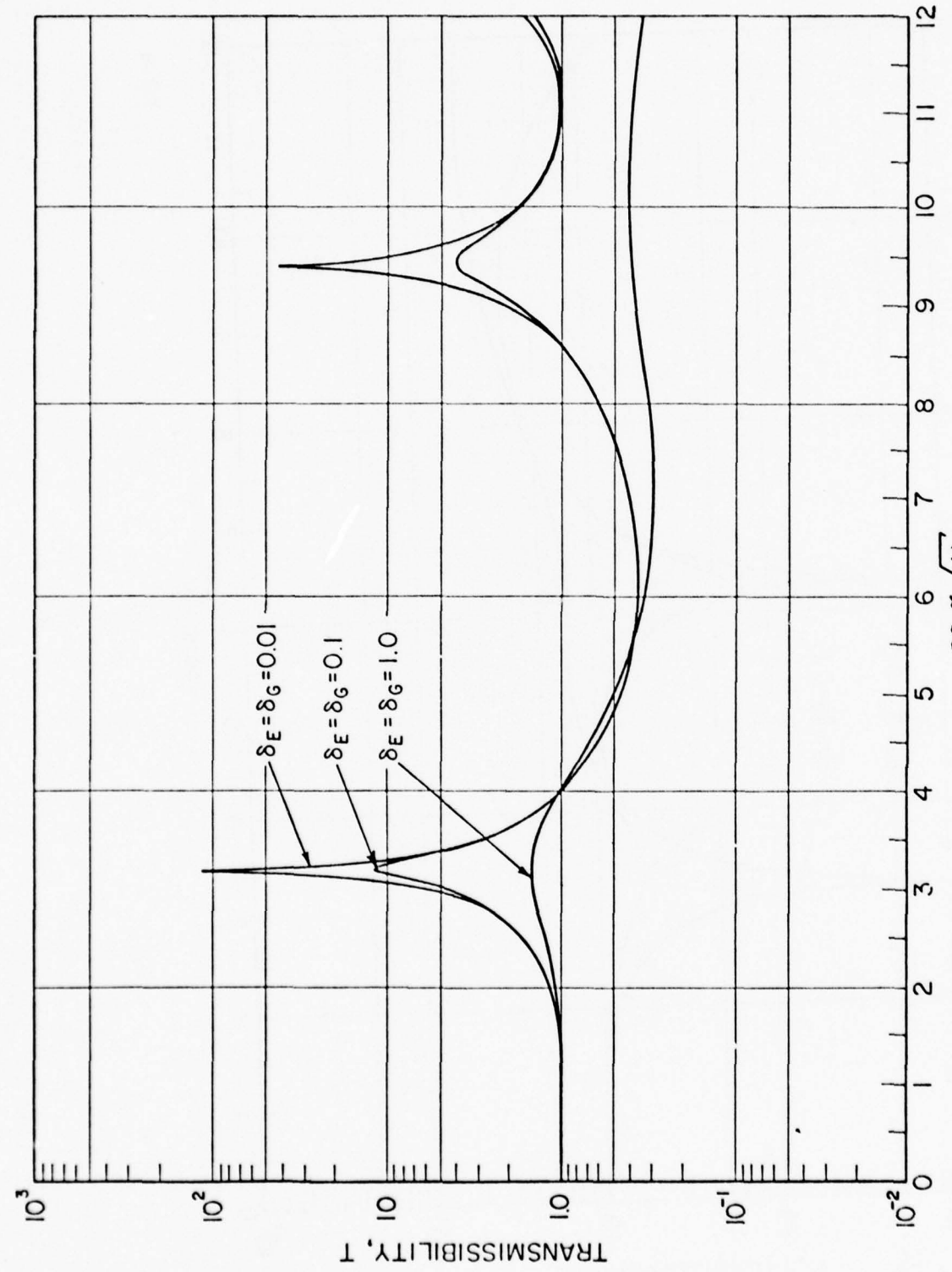
TRANSMISSIBILITY, T
10^{3}
10^{2}
10
1
10^{-1}
10^{-2}
0
1
2
3
4
5
6
7
8
9
10
11
12
$\delta_E=\delta_G=0.01$
$\delta_E=\delta_G=0.1$
$\delta_E=\delta_G=1.0$
$n a \alpha \sqrt{\omega}$

FIG. 5

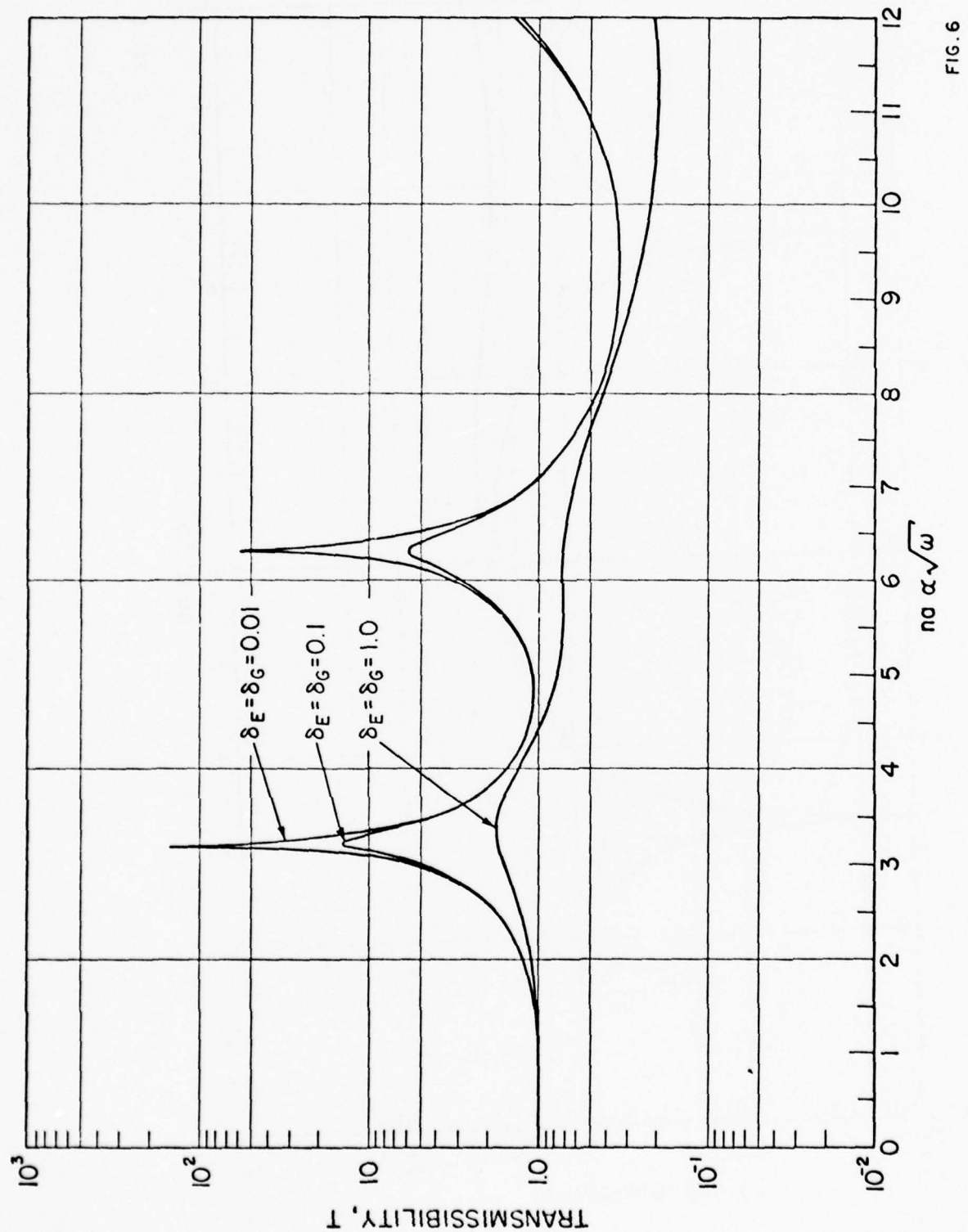
TRANSMISSIBILITY, T
10^3
10^2
10
1.0
10^{-1}
10^{-2}
0
1
2
3
4
5
6
7
8
9
10
11
12
$\delta_E=\delta_G=0.01$
$\delta_E=\delta_G=0.1$
$\delta_E=\delta_G=1.0$
$n\alpha\sqrt{\omega}$

FIG. 6

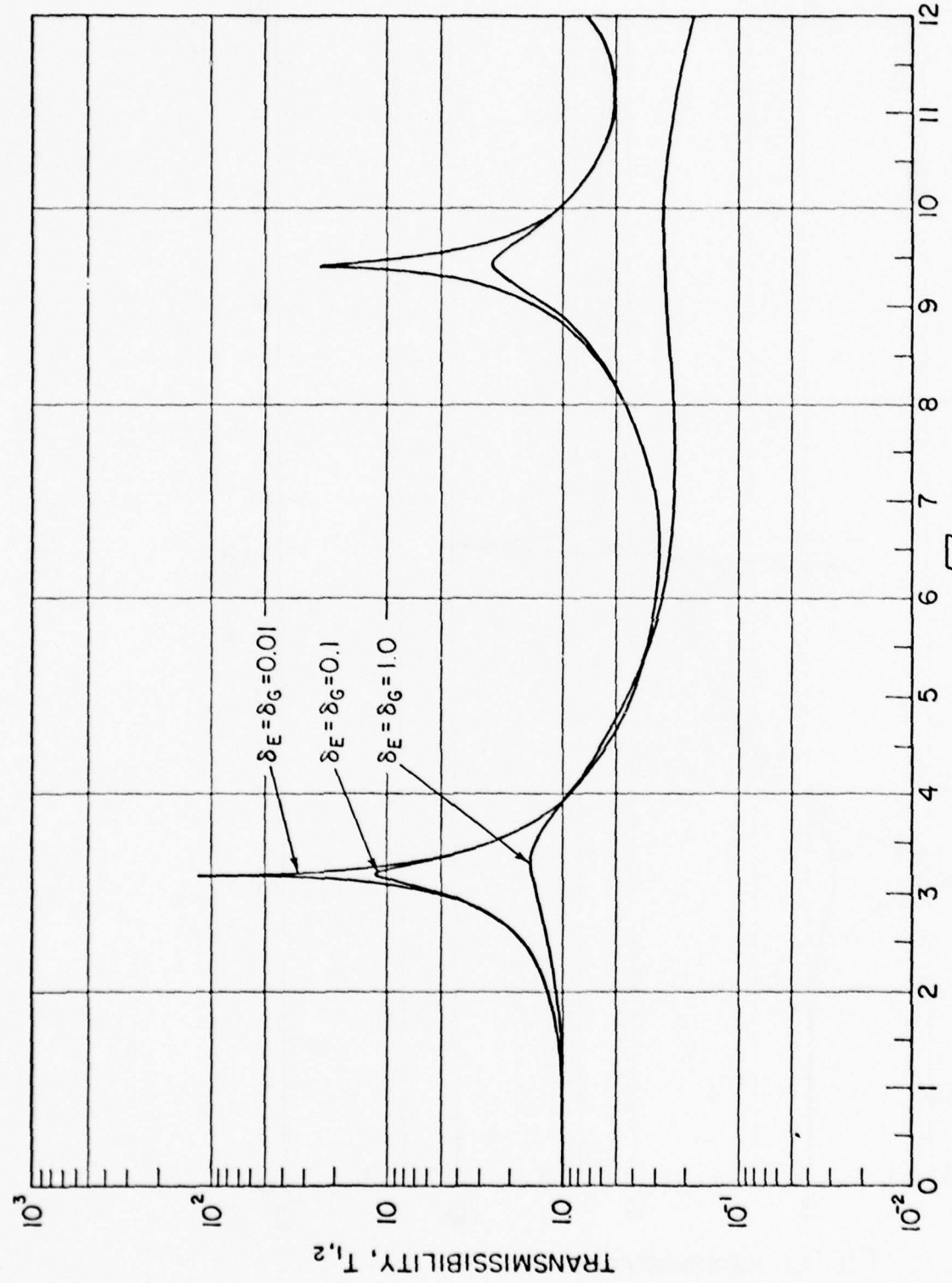
TRANSMISSIBILITY, $T_{1,2}$
10^3
10^2
10
1.0
10^{-1}
10^{-2}
0
1
2
3
4
5
6
7
8
9
10
11
12
$na\,\alpha\sqrt{\omega}$
$\delta_E=\delta_G=0.01$
$\delta_E=\delta_G=0.1$
$\delta_E=\delta_G=1.0$

FIG.7

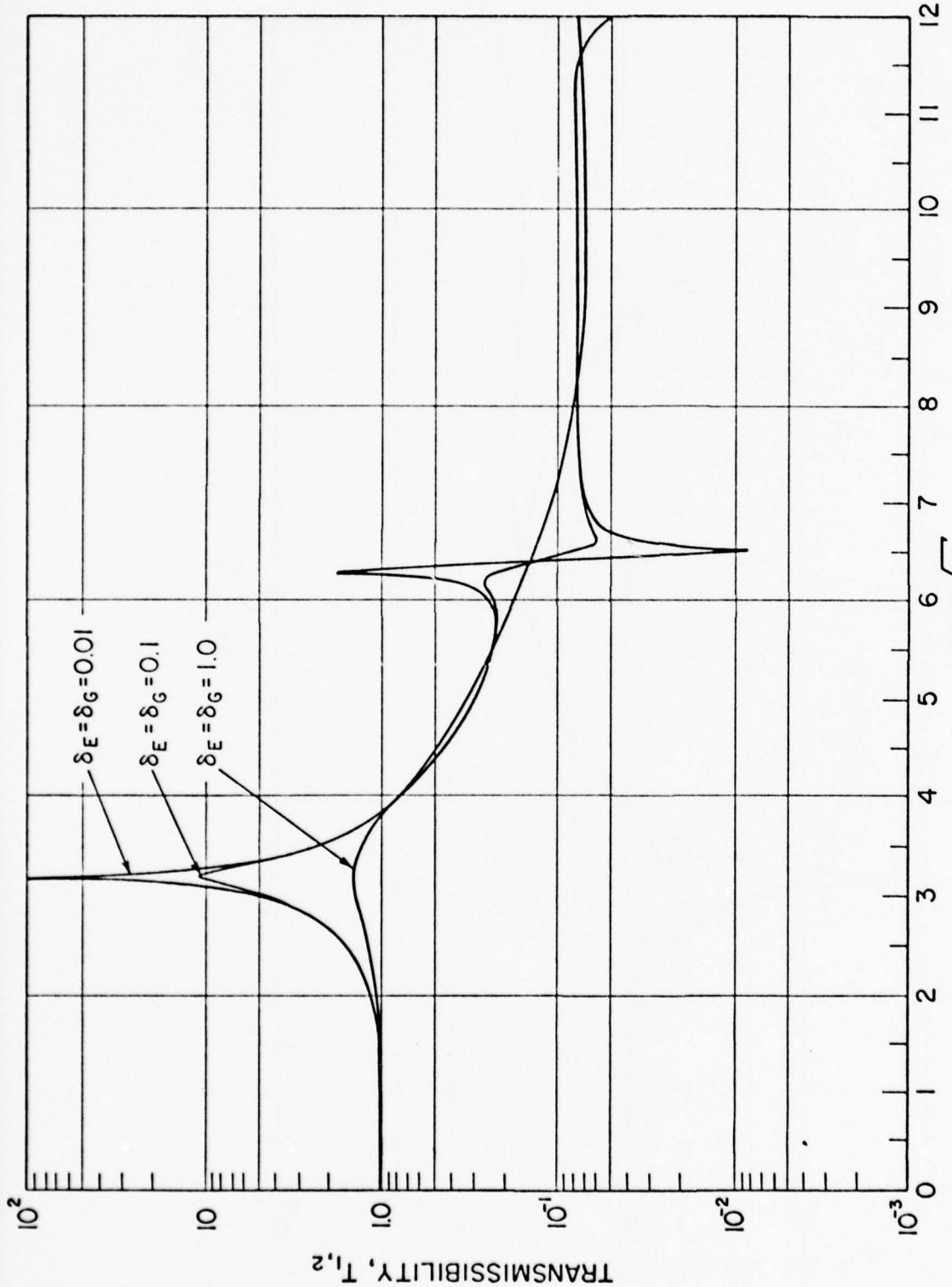
TRANSMISSIBILITY, $T_{1,2}$
10^{2}
10
1.0
10^{-1}
10^{-2}
10^{-3}
0
1
2
3
4
5
6
7
8
9
10
11
12
$n\alpha\sqrt{\omega}$
$\delta_E=\delta_G=0.01$
$\delta_E=\delta_G=0.1$
$\delta_E=\delta_G=1.0$

FIG. 8

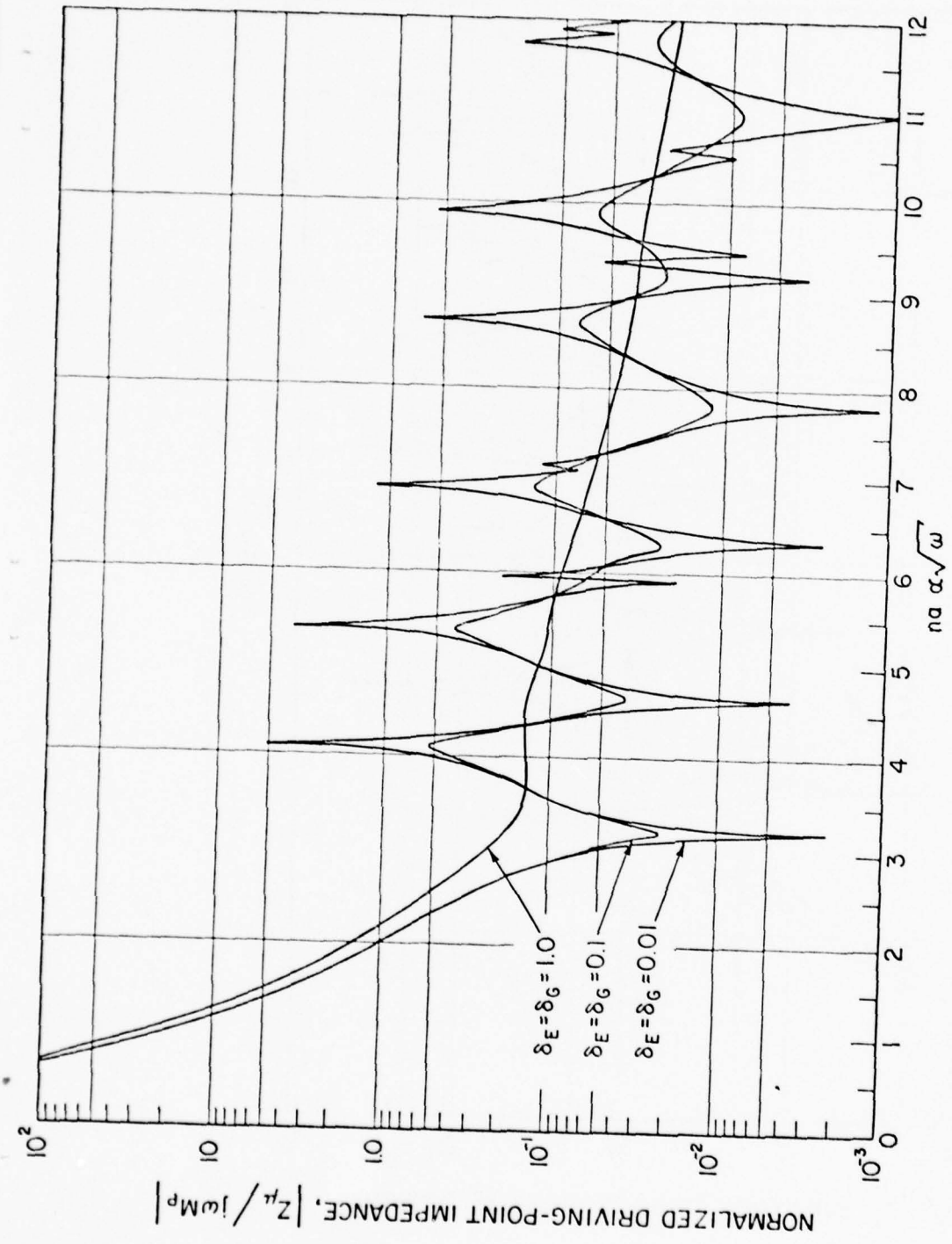
NORMALIZED DRIVING-POINT IMPEDANCE, $|Z_{\mu\mu}/j\omega M_p|$
10^2
10
1.0
10^{-1}
10^{-2}
10^{-3}
0
1
2
3
4
5
6
7
8
9
10
11
12
$na\alpha\sqrt{\omega}$
$\delta_E=\delta_G=1.0$
$\delta_E=\delta_G=0.1$
$\delta_E=\delta_G=0.01$

FIG. 9

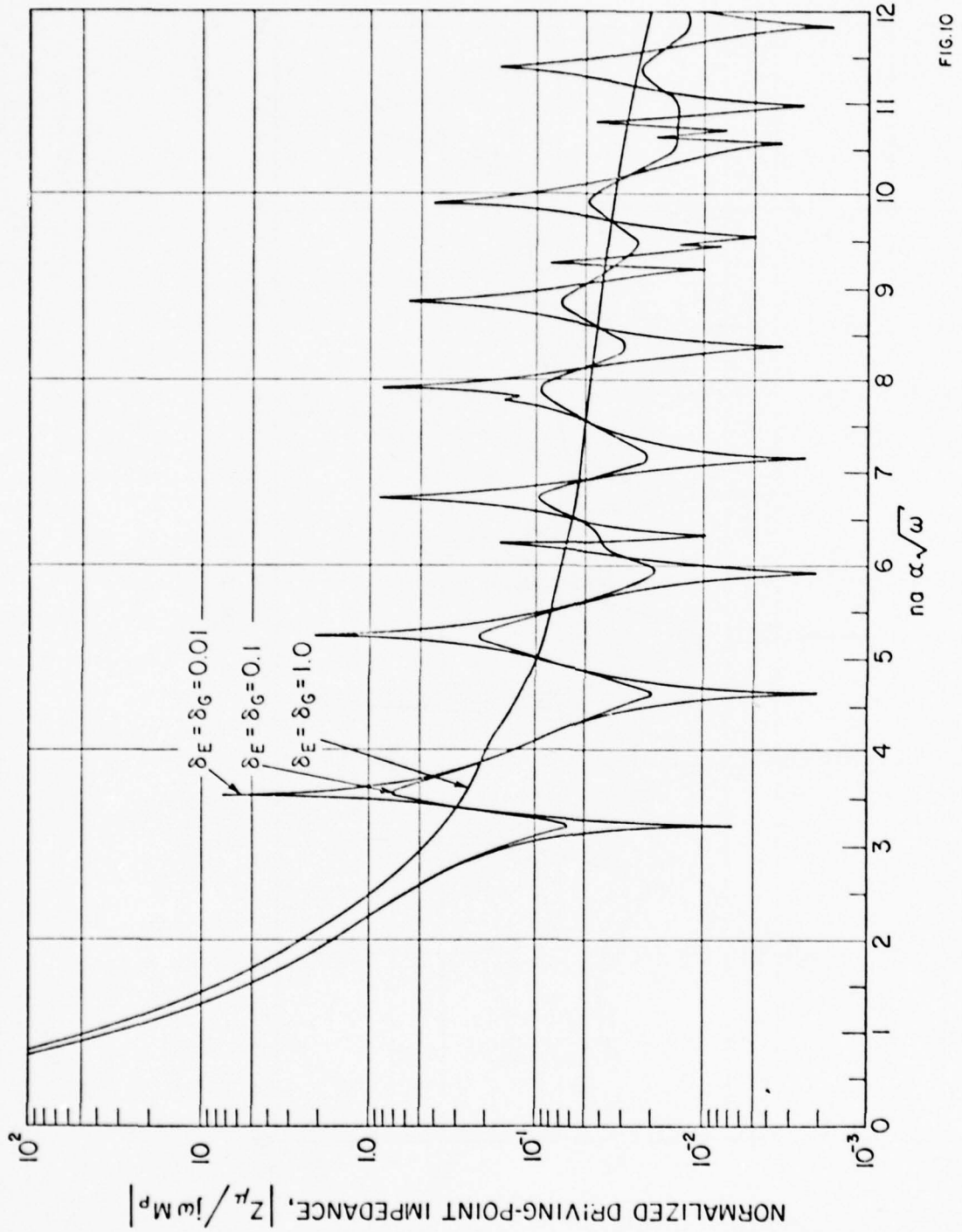
NORMALIZED DRIVING-POINT IMPEDANCE, $|Z_{\mu}/j\omega M_{\rho}|$
10^{2}
10
1.0
10^{-1}
10^{-2}
10^{-3}
0
1
2
3
4
5
6
7
8
9
10
11
12
$na\alpha\sqrt{\omega}$
$\delta_E = \delta_G = 0.01$
$\delta_E = \delta_G = 0.1$
$\delta_E = \delta_G = 1.0$

FIG.10

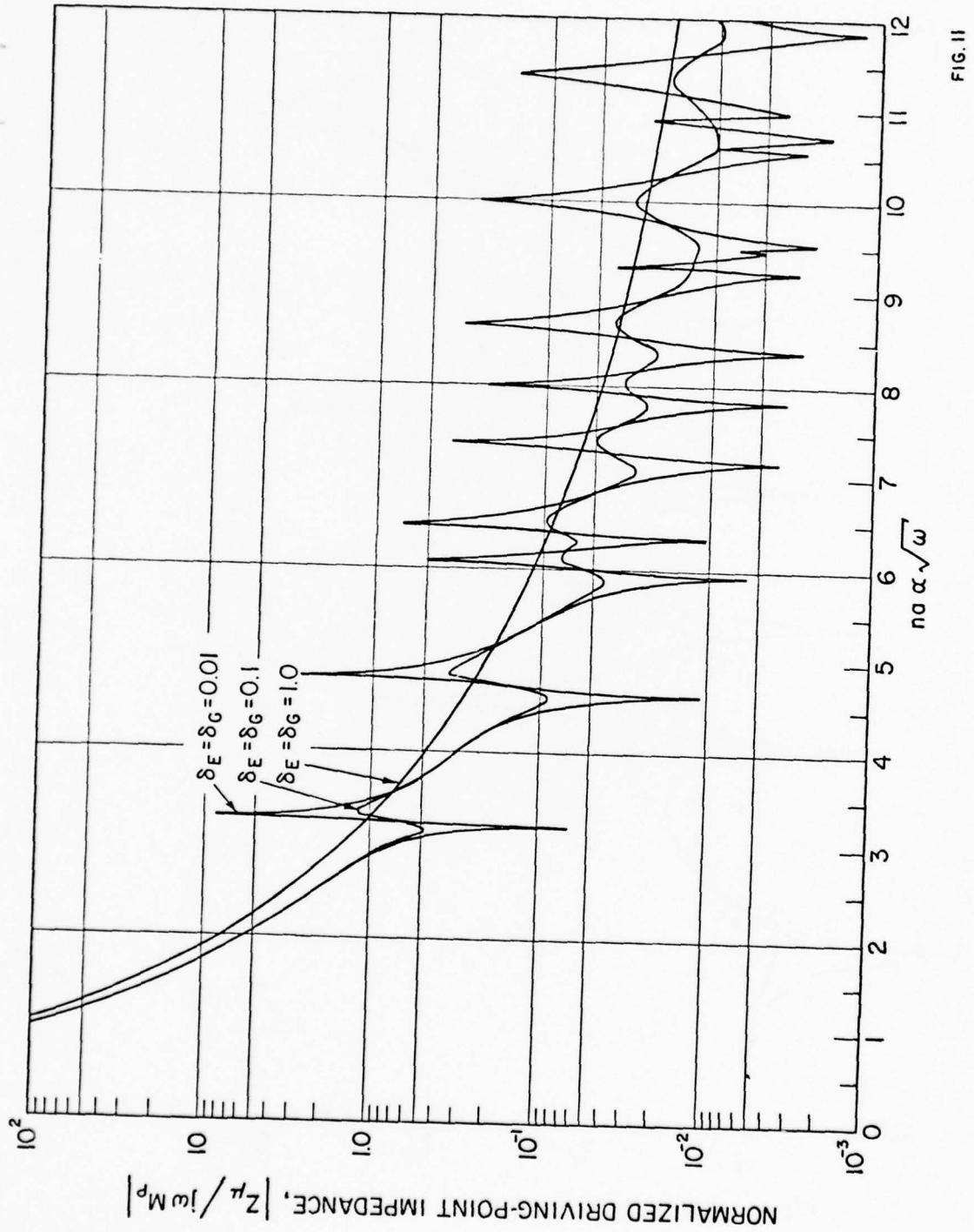
NORMALIZED DRIVING-POINT IMPEDANCE, $|Z_{pp}/j\omega M_p|$
10^2
10
1.0
10^{-1}
10^{-2}
10^{-3}
0
1
2
3
4
5
6
7
8
9
10
11
12
$na\alpha\sqrt{\omega}$
$\delta_E=\delta_G=0.01$
$\delta_E=\delta_G=0.1$
$\delta_E=\delta_G=1.0$

FIG. 11

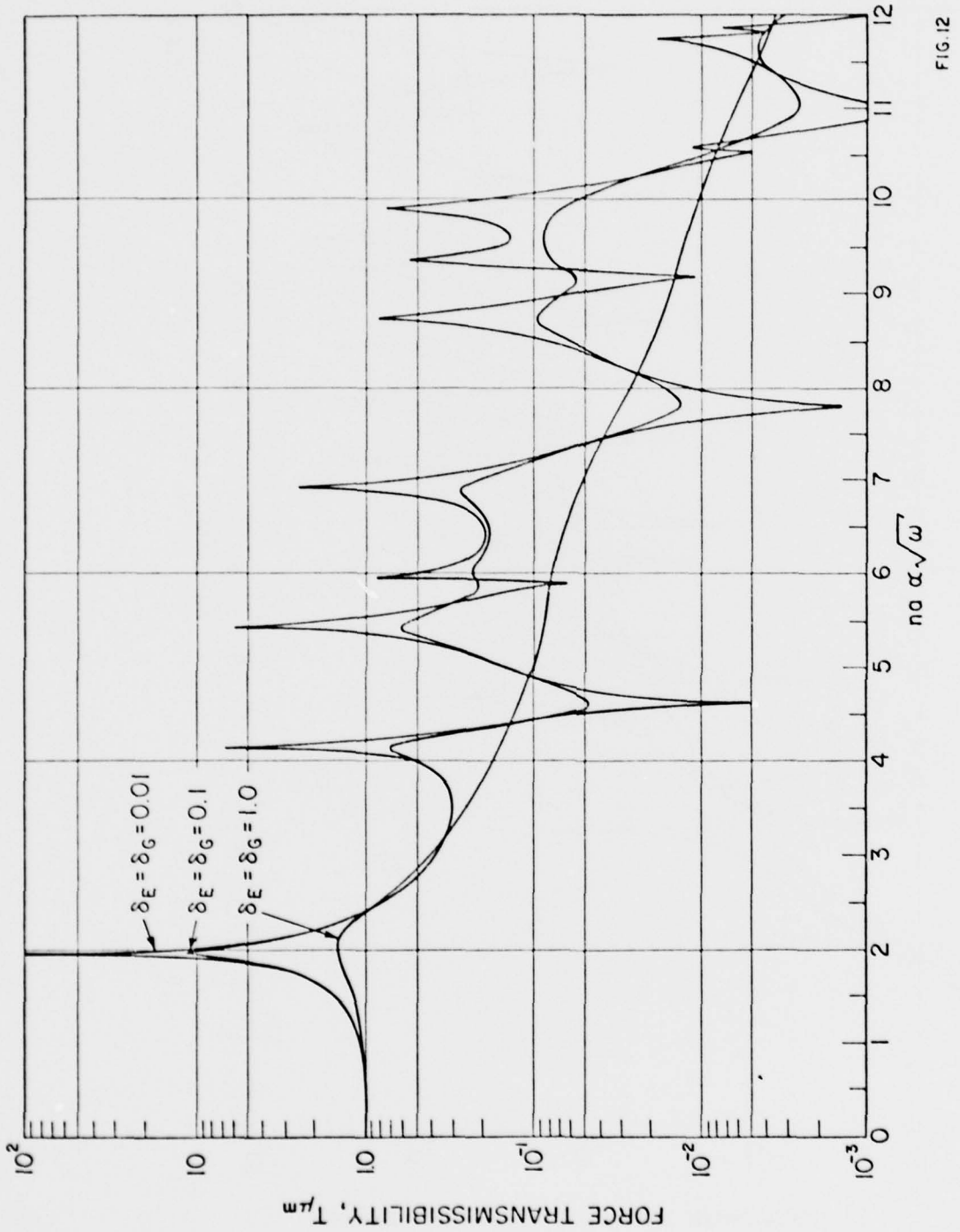
FORCE TRANSMISSIBILITY, $T_{\mu m}$
10^{2}
10
1
10^{-1}
10^{-2}
10^{-3}
0
1
2
3
4
5
6
7
8
9
10
11
12
$n\alpha\sqrt{\omega}$
$\delta_E = \delta_G = 0.01$
$\delta_E = \delta_G = 0.1$
$\delta_E = \delta_G = 1.0$

FIG.12

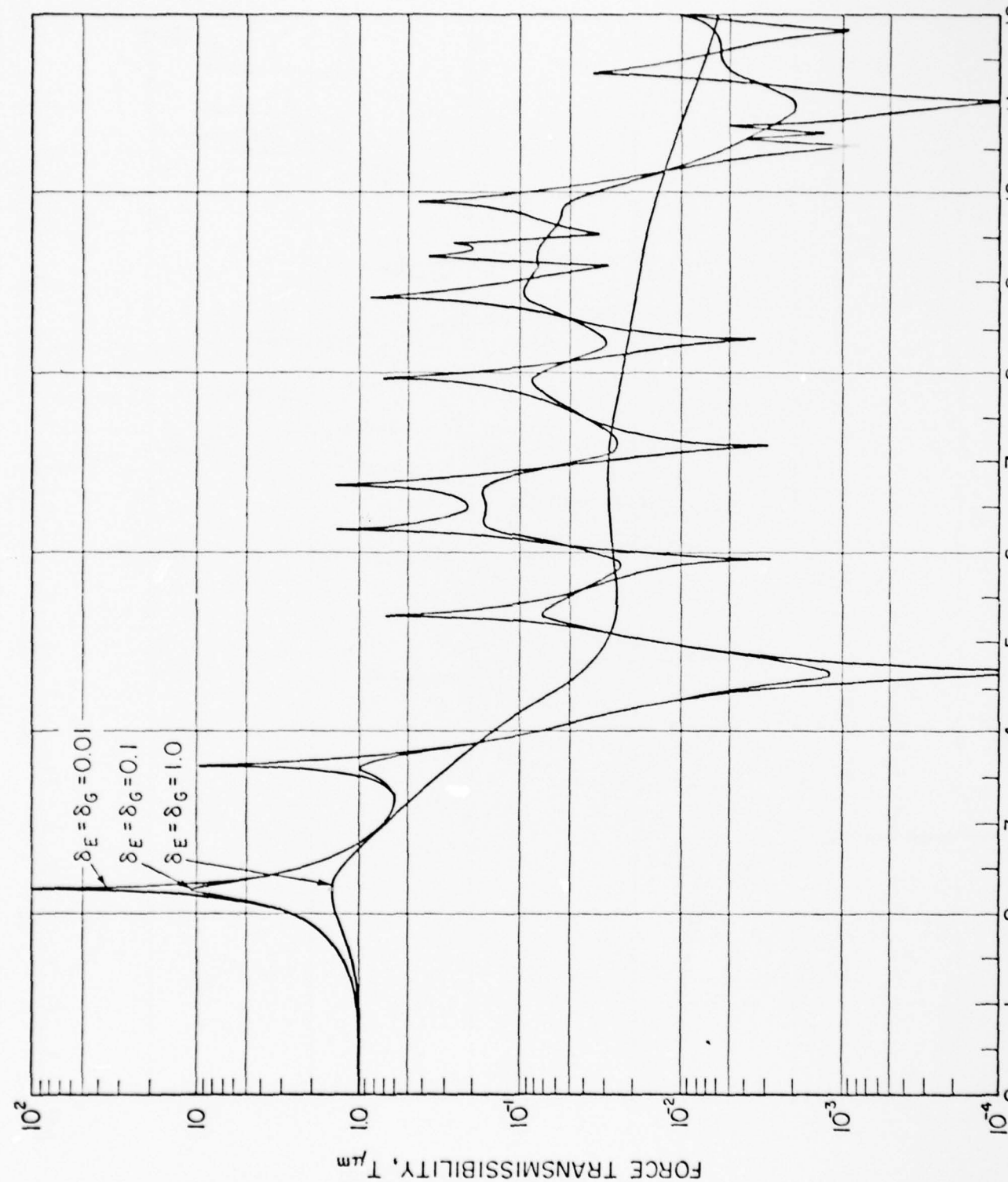
FORCE TRANSMISSIBILITY, $T_{\mu m}$
10^{2}
10
1
10^{-1}
10^{-2}
10^{-3}
10^{-4}
0
1
2
3
4
5
6
7
8
9
10
11
12
$n a \alpha \sqrt{\omega}$
$\delta_E = \delta_G = 0.01$
$\delta_E = \delta_G = 0.1$
$\delta_E = \delta_G = 1.0$

FIG. 13

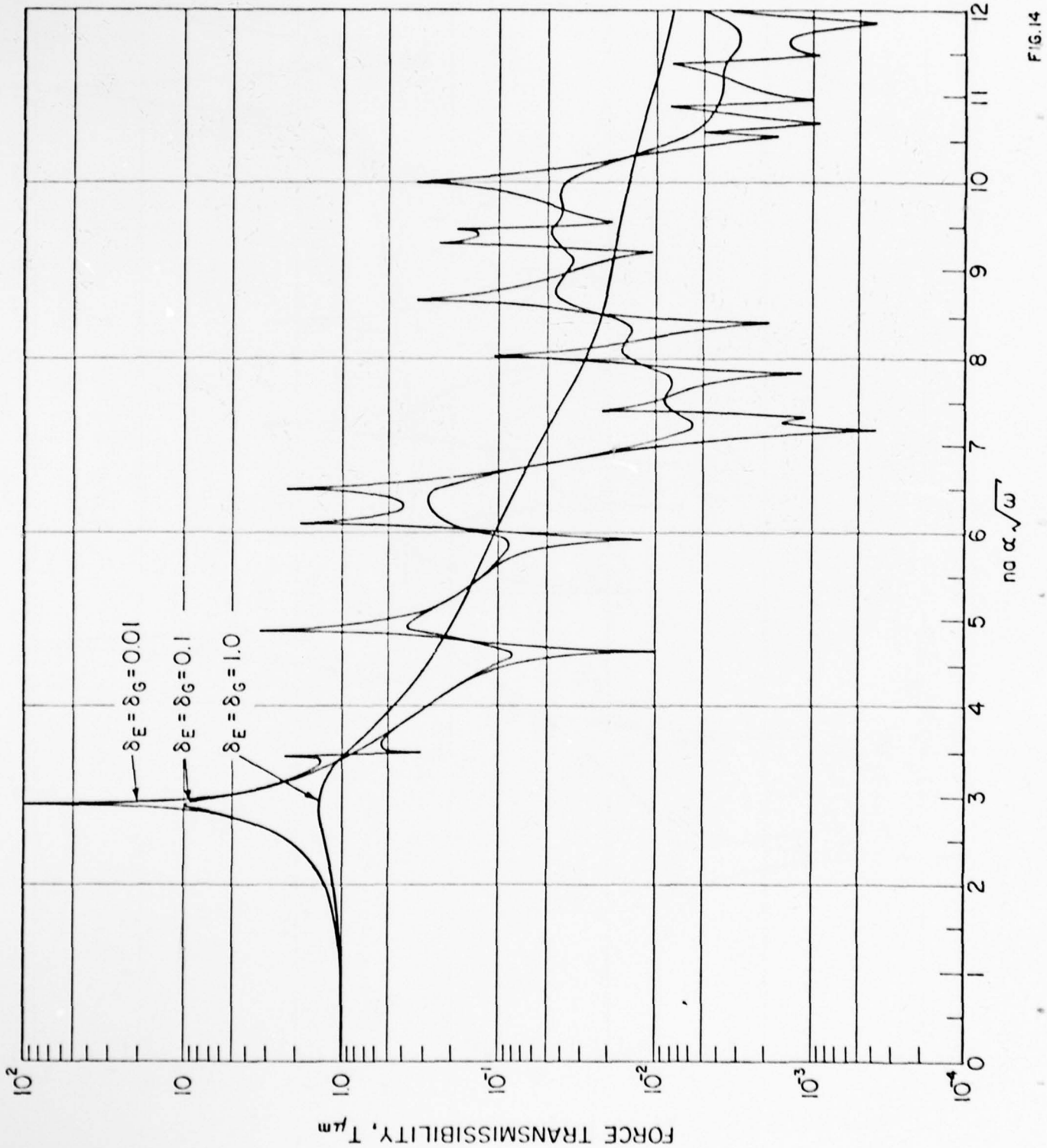
FORCE TRANSMISSIBILITY, $T_{\mu m}$
10^{-4}
10^{-3}
10^{-2}
10^{-1}
1.0
10
10^{2}
0
1
2
3
4
5
6
7
8
9
10
11
12
$\eta a \alpha \sqrt{\omega}$
$\delta_E = \delta_G = 0.001$
$\delta_E = \delta_G = 0.1$
$\delta_E = \delta_G = 1.0$

FIG. 14

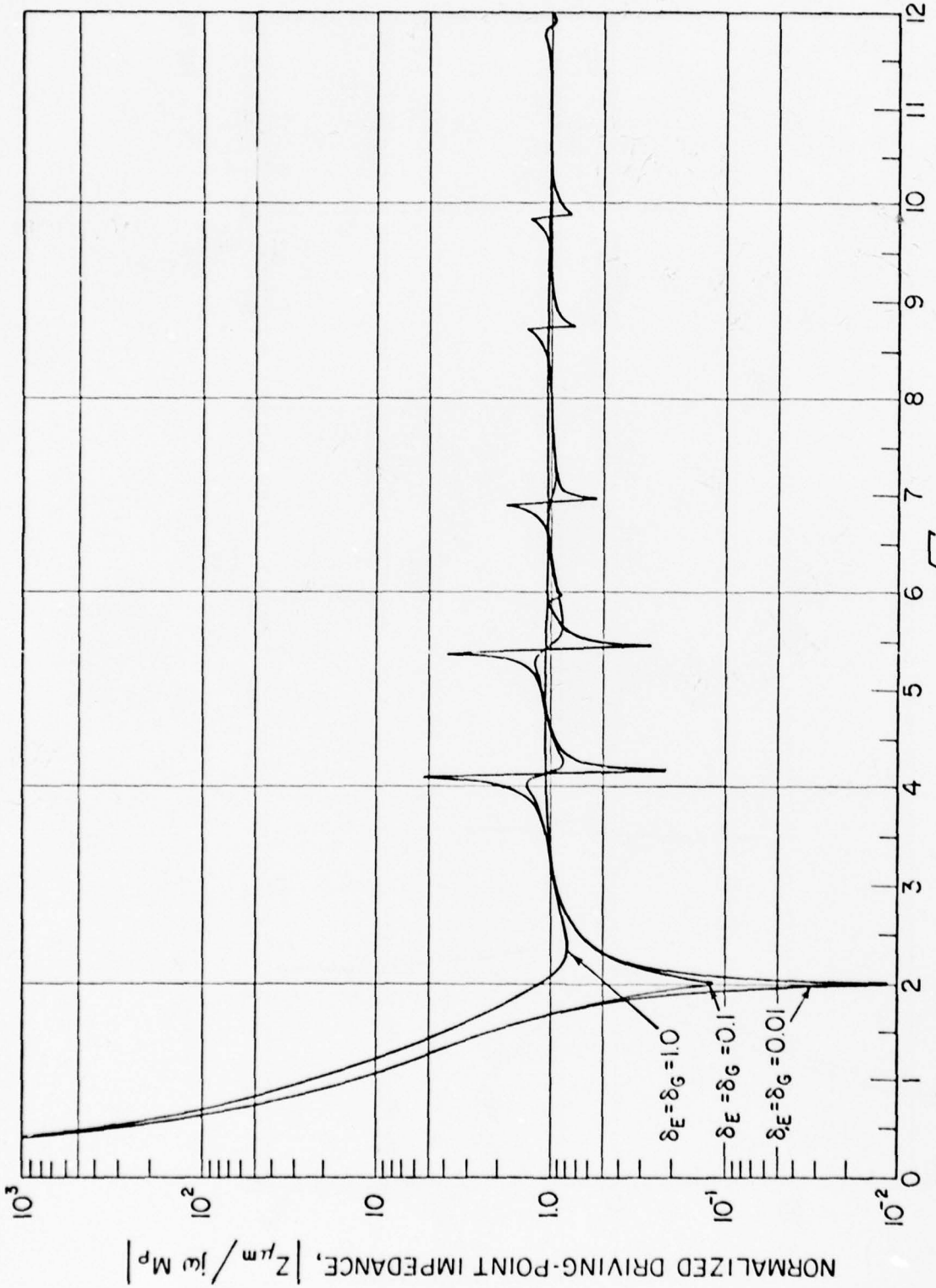
NORMALIZED DRIVING-POINT IMPEDANCE, $|Z_{\mu\mu}/j\omega M_p|$
10^3
10^2
10
1.0
10^{-1}
10^{-2}
0
1
2
3
4
5
6
7
8
9
10
11
12
$na\alpha\sqrt{\omega}$
$\delta_E=\delta_G=1.0$
$\delta_E=\delta_G=0.1$
$\delta_E=\delta_G=0.01$

FIG.15

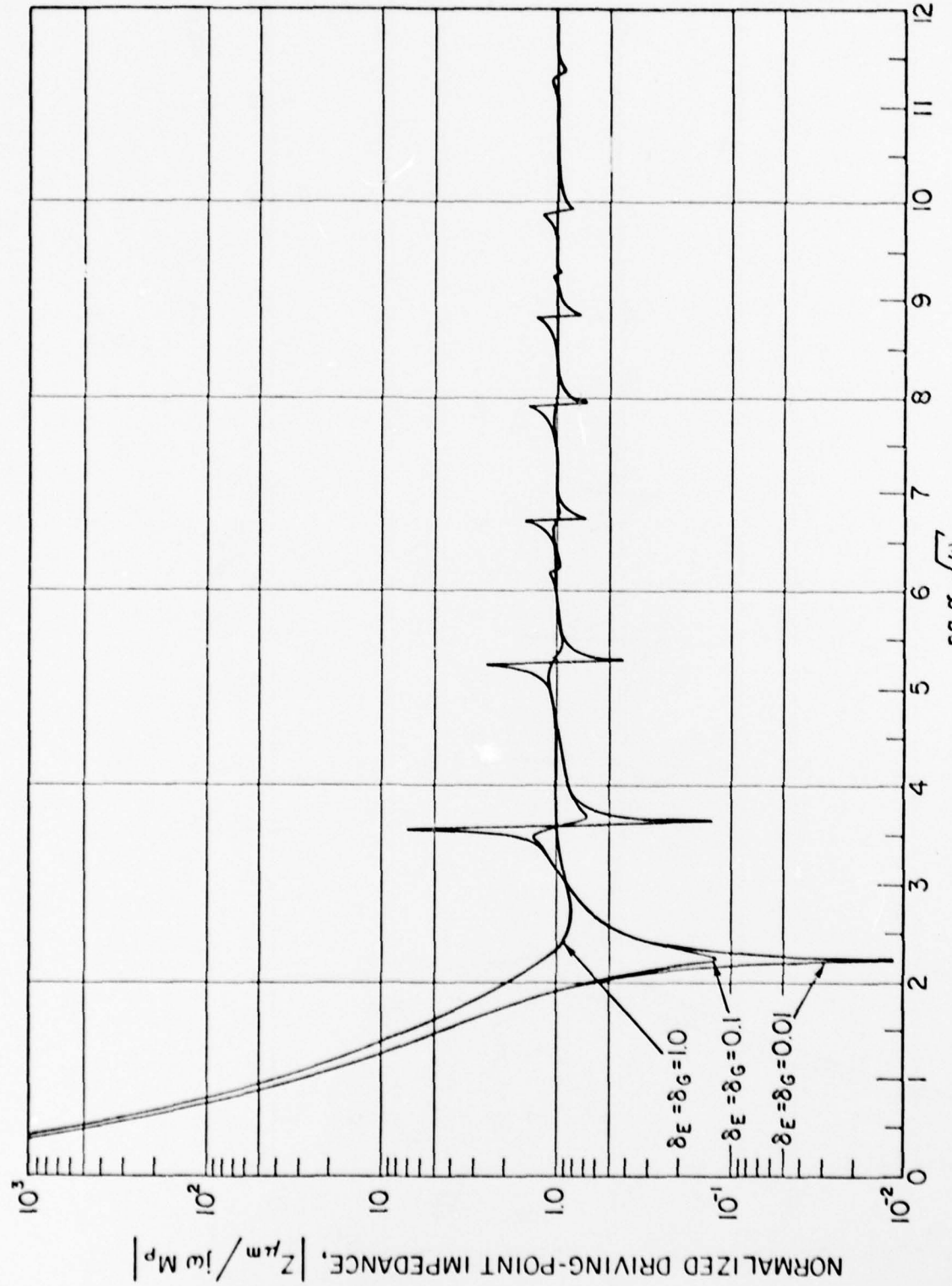
NORMALIZED DRIVING-POINT IMPEDANCE, $\left|Z_{\mu\mu}/j\omega M_p\right|$
10^3
10^2
10
1.0
10^{-1}
10^{-2}
0
1
2
3
4
5
6
7
8
9
10
11
12
$na\alpha\sqrt{\omega}$
$\delta_E=\delta_G=1.0$
$\delta_E=\delta_G=0.1$
$\delta_E=\delta_G=0.01$

FIG. 16

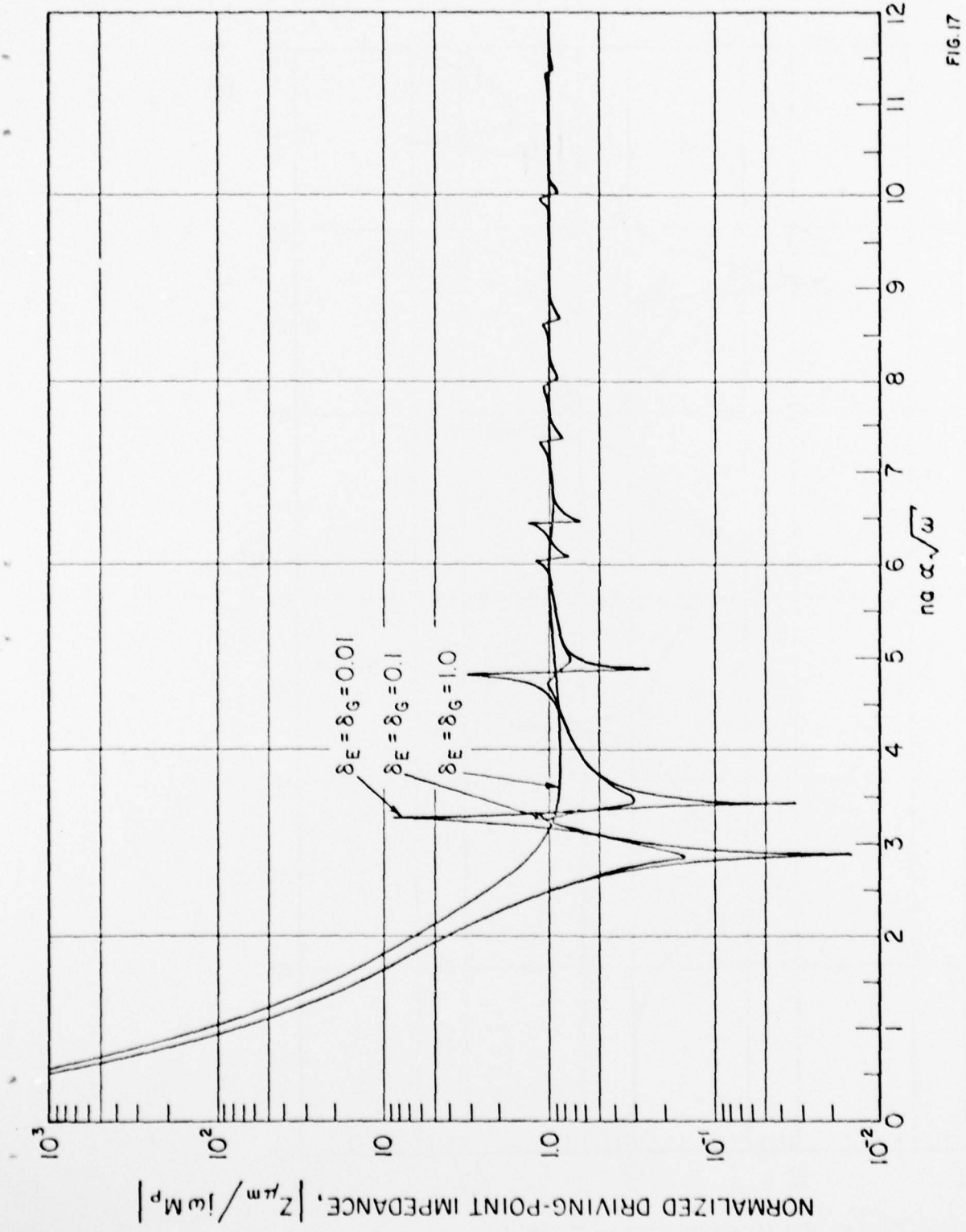
NORMALIZED DRIVING-POINT IMPEDANCE, $|Z_{\mu\mu}/j\omega M_p|$
10^3
10^2
10
1.0
10^{-1}
10^{-2}
0
1
2
3
4
5
6
7
8
9
10
11
12
$na\alpha\sqrt{\omega}$
$\delta_E = \delta_G = 0.01$
$\delta_E = \delta_G = 0.1$
$\delta_E = \delta_G = 1.0$

FIG. 17

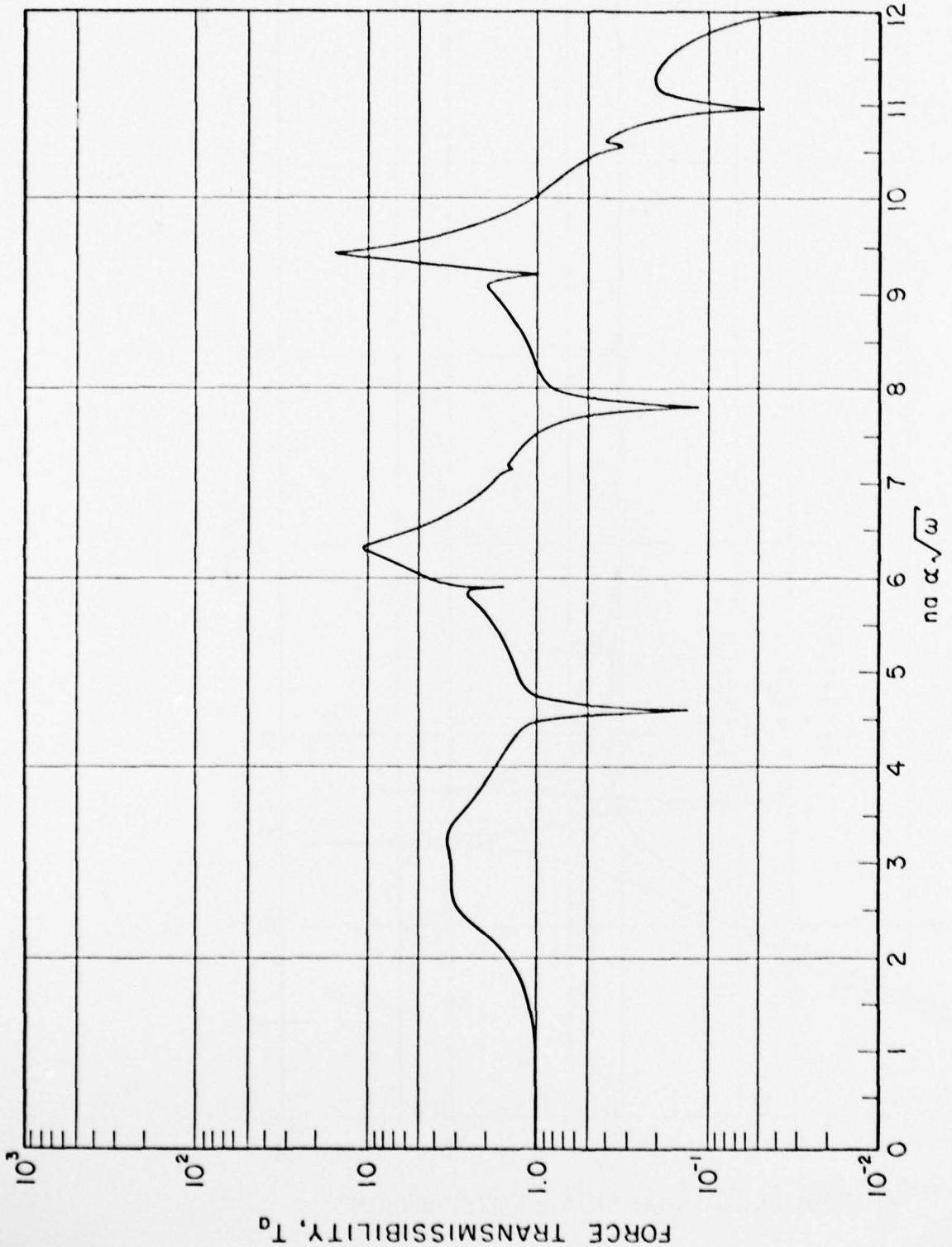
FORCE TRANSMISSIBILITY, T_a
10^3
10^2
10
1.0
10^{-1}
10^{-2}
0
1
2
3
4
5
6
7
8
9
10
11
12
$na\alpha\sqrt{\omega}$

FIG. 18

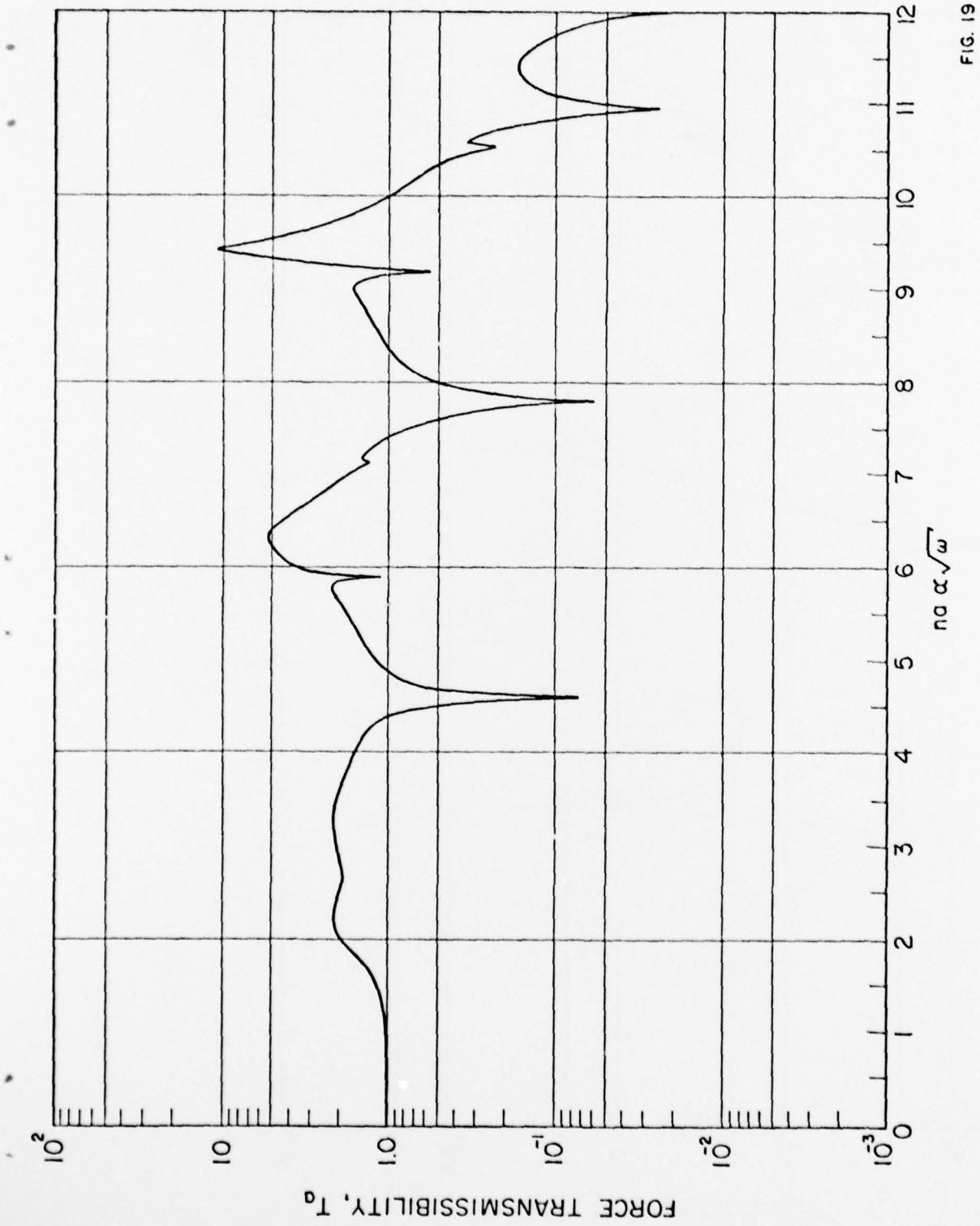
FORCE TRANSMISSIBILITY, T_a
10^2
10
1
10^{-1}
10^{-2}
10^{-3}
0
1
2
3
4
5
6
7
8
9
10
11
12
$na\alpha\sqrt{\omega}$

FIG. 19

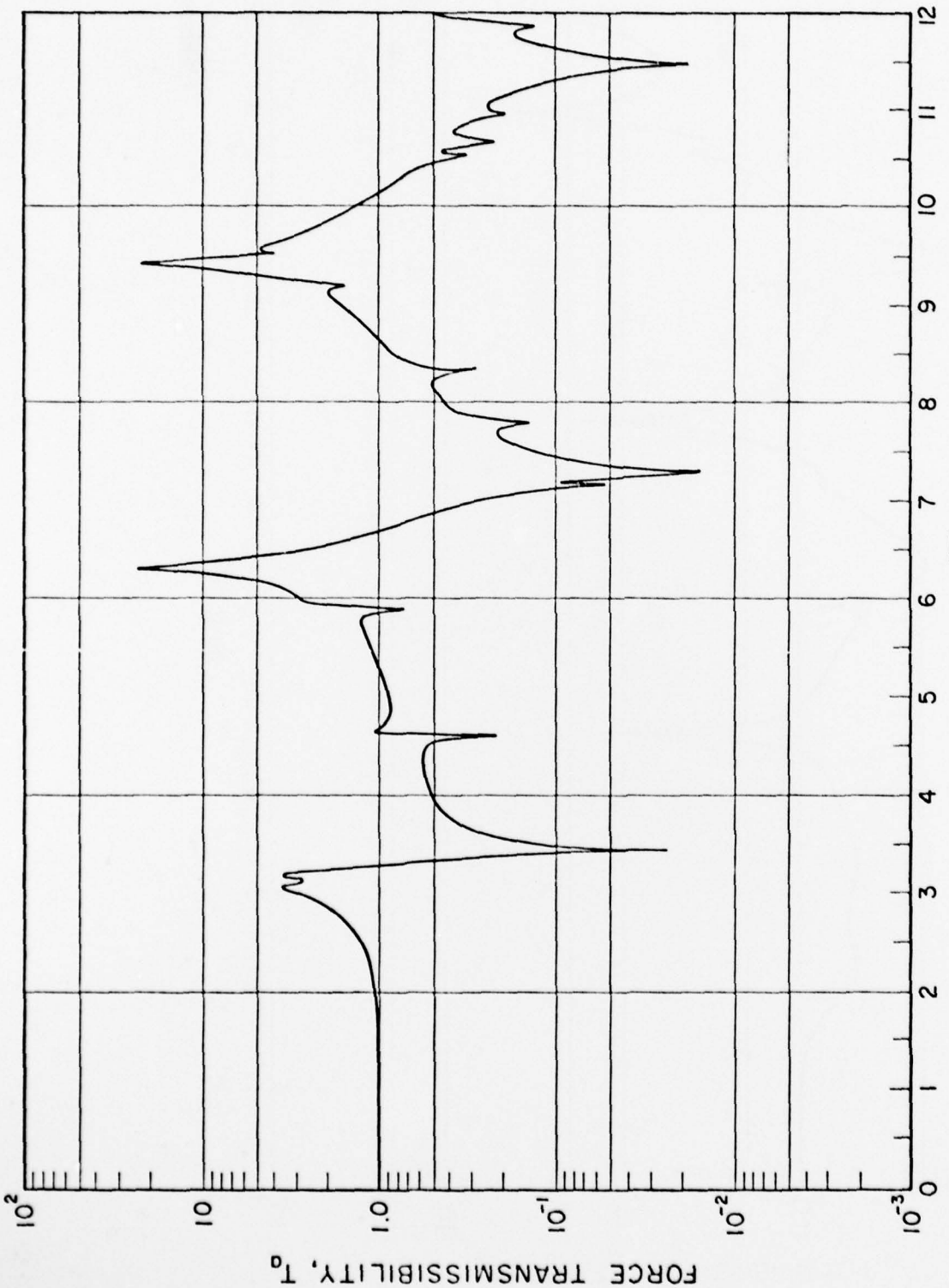
FORCE TRANSMISSIBILITY, T_a
10^2
10
1.0
10^{-1}
10^{-2}
10^{-3}
0
1
2
3
4
5
6
7
8
9
10
11
12
$\eta a \propto \sqrt{\omega}$

FIG. 20

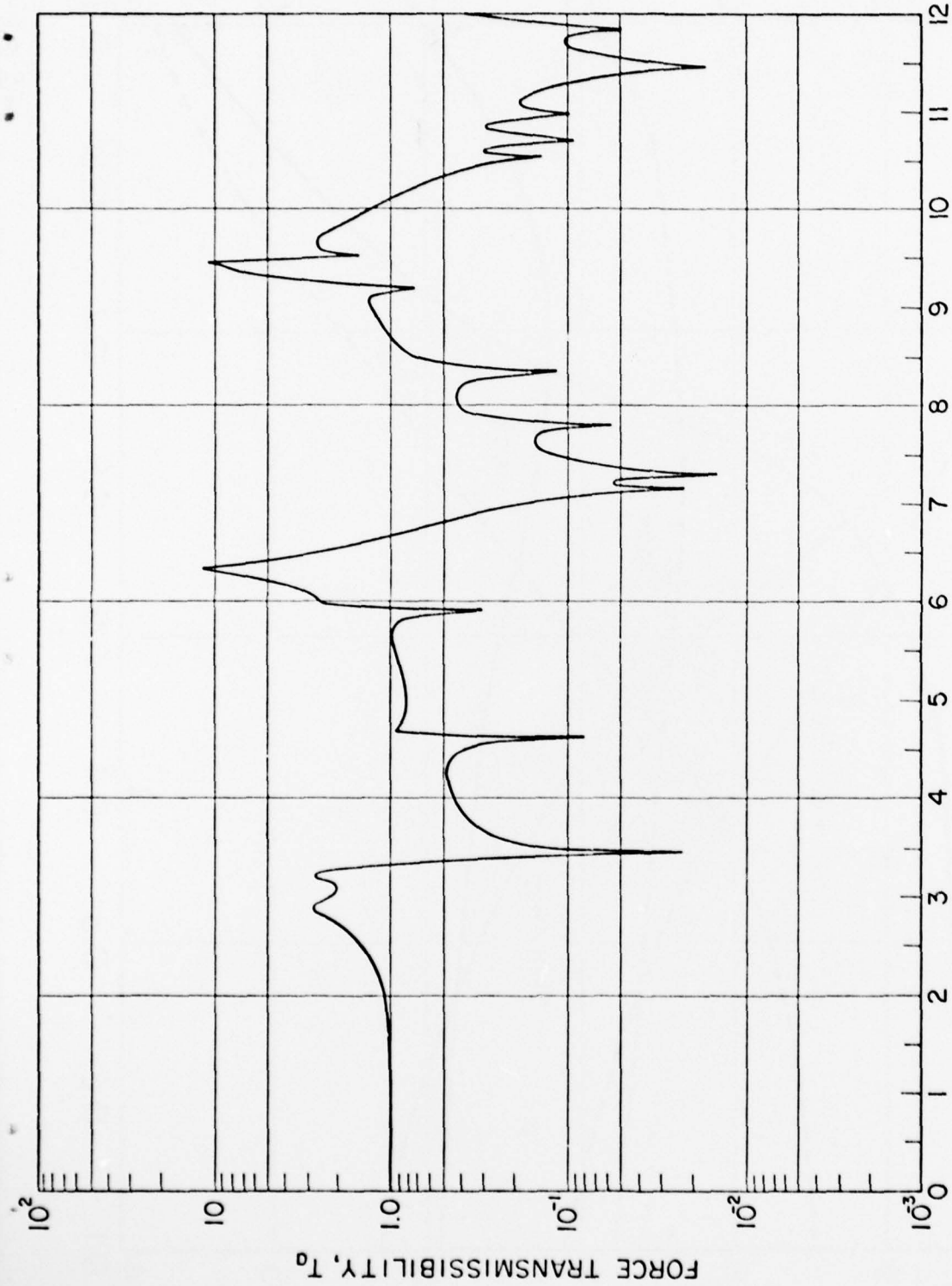
FORCE TRANSMISSIBILITY, T_a
10^2
10
1.0
10^{-1}
10^{-2}
10^{-3}
0
1
2
3
4
5
6
7
8
9
10
11
12
$na\alpha\sqrt{\omega}$

FIG. 21

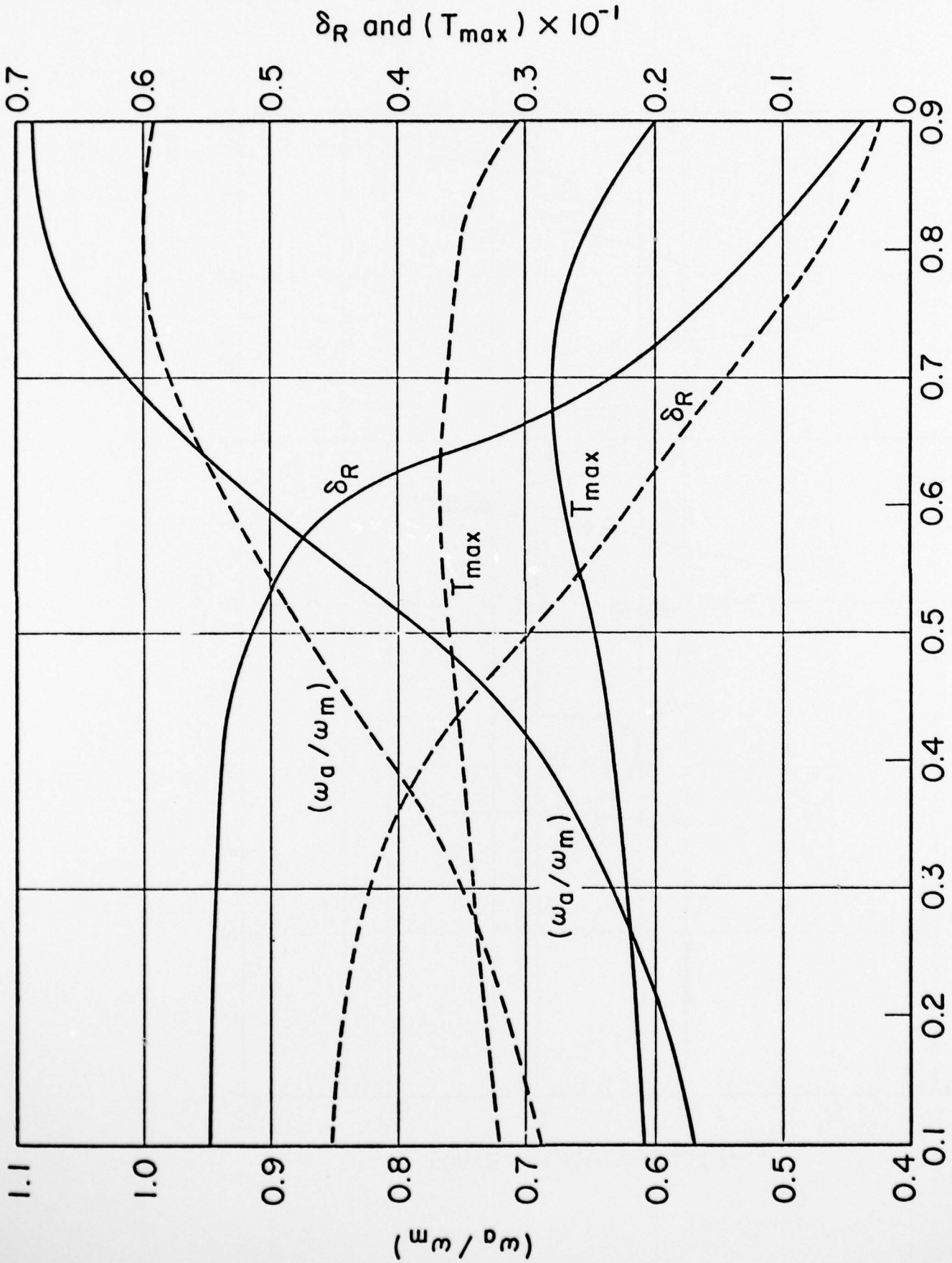
δ_R and $(T_{max}) \times 10^{-1}$
0.7
0.6
0.5
0.4
0.3
0.2
0.1
0
0.9
0.8
0.7
0.6
0.5
0.4
0.3
0.2
0.1
μ
δ_R
T_{max}
T_{max}
δ_R
(ω_a/ω_m)
(ω_a/ω_m)
1.1
1.0
0.9
0.8
0.7
0.6
0.5
0.4
(ω_a/ω_m)

FIG. 22

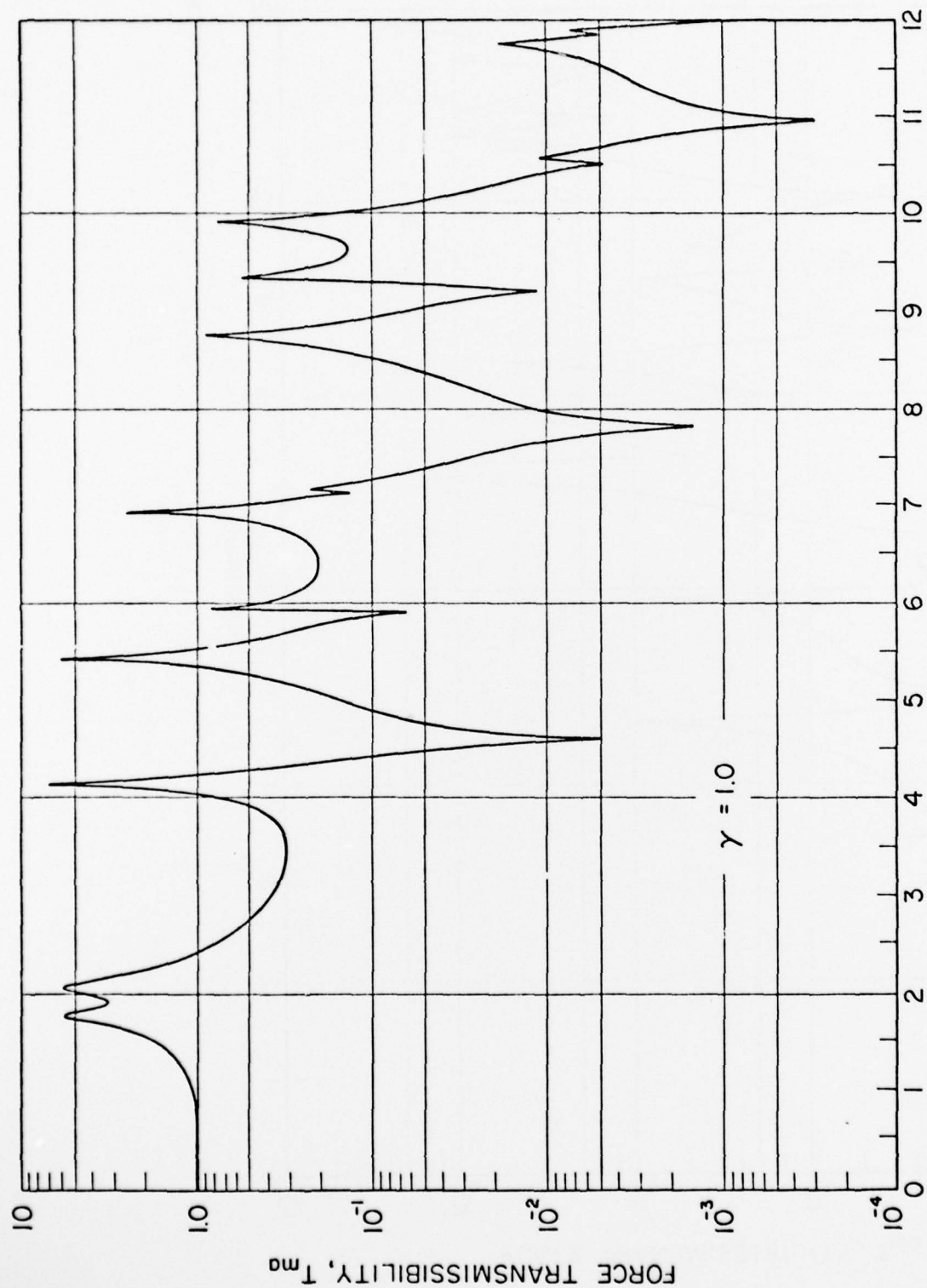
FORCE TRANSMISSIBILITY, T_{ma}
10
1.0
10^{-1}
10^{-2}
10^{-3}
10^{-4}
0
1
2
3
4
5
6
7
8
9
10
11
12
$\gamma = 1.0$
$\eta\alpha \propto \sqrt{\omega}$

FIG. 23

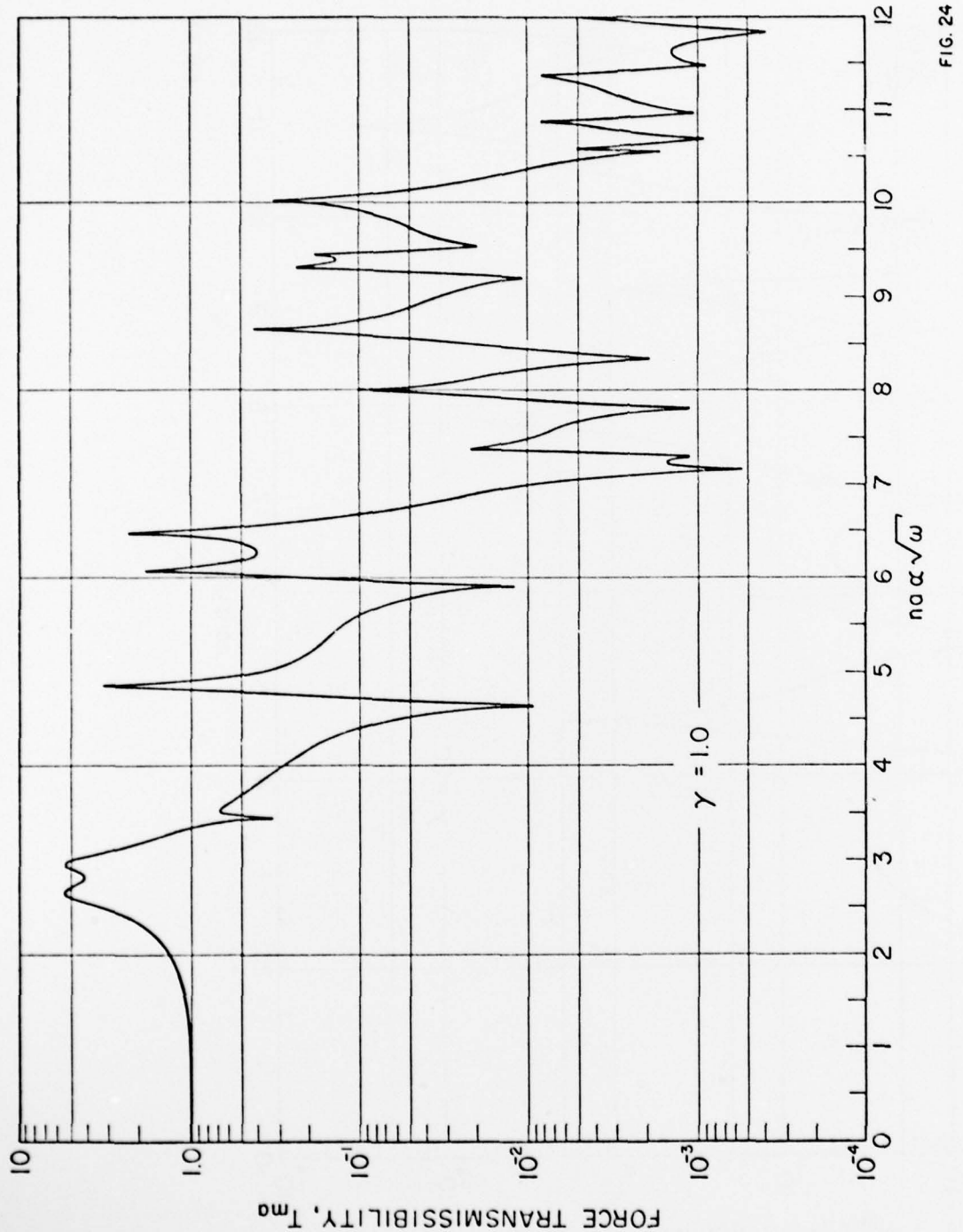
FORCE TRANSMISSIBILITY, T_{ma}
10
1.0
10^{-1}
10^{-2}
10^{-3}
10^{-4}
0
1
2
3
4
5
6
7
8
9
10
11
12
$\gamma = 1.0$
$n\alpha\sqrt{\omega}$

FIG. 24

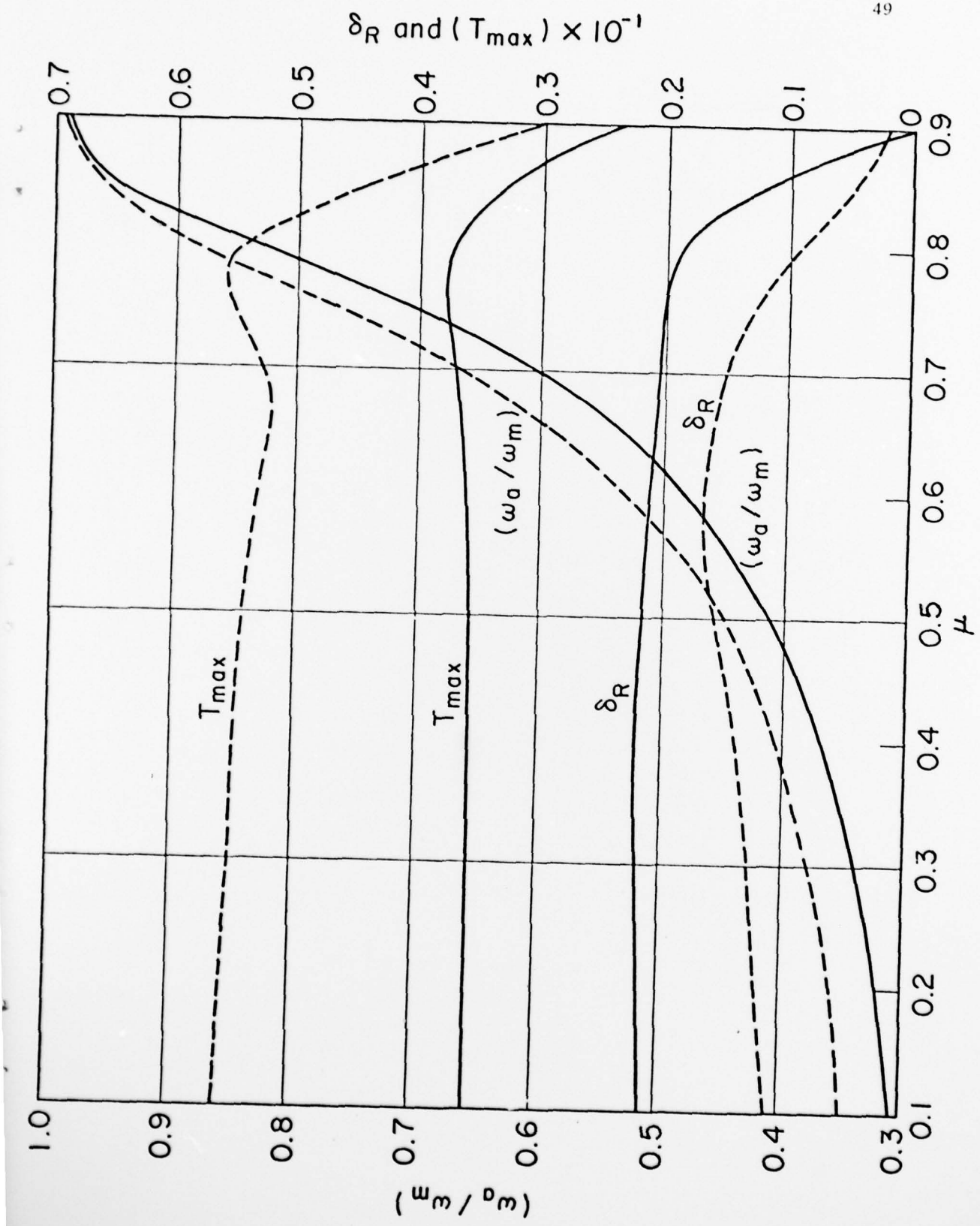
δR and (Tmax) × 10⁻¹
0.7
0.6
0.5
0.4
0.3
0.2
0.1
0
0.9
0.8
0.7
0.6
0.5
0.4
0.3
0.2
0.1
μ
Tmax
Tmax
δR
δR
(ωa / ωm)
(ωa / ωm)
1.0
0.9
0.8
0.7
0.6
0.5
0.4
0.3
(ωa / ωm)

FIG. 25

Commander
Naval Sea Systems Command
Department of the Navy
Washington, D.C. 20362
Attn: Mr. Stephen M. Blazek
SEA 05HB
(Copy Nos. 1,2,3,4)

Commander
Naval Sea Systems Command
Department of the Navy
Washington, D.C. 20362
Attn: Mr. C. C. Taylor
SEA 05H3
(Copy Nos. 5 and 6)

Commander
Naval Sea Systems Command
Department of the Navy
Washington, D.C. 20362
Attn: SEA 921N
(Copy No. 7)

Commander
Naval Sea Systems Command
Department of the Navy
Washington, D.C. 20362
Attn: PMS 393
(Copy No. 8)

Commander
Naval Sea Systems Command
Department of the Navy
Washington, D.C. 20362
Attn: PMS 395
(Copy No. 9)

Commander
Naval Sea Systems Command
Department of the Navy
Washington, D.C. 20362
Attn: PMS 396
(Copy No. 10)

Commander
Naval Sea Systems Command
Department of the Navy
Washington, D.C. 20362
Attn: SEA 6103
(Copy Nos. 11 and 12)

Commander
Naval Sea Systems Command
Department of the Navy
Washington, D.C. 20362
Attn: SEA 322
(Copy No. 13)

Commander
Naval Sea Systems Command
Department of the Navy
Washington, D.C. 20362
Attn: SEA 3221
(Copy No. 14)

Commander
Naval Sea Systems Command
Department of the Navy
Washington, D.C. 20362
Attn: SEA 3222
(Copy No. 15)

Commander
Naval Sea Systems Command
Department of the Navy
Washington, D.C. 20362
Attn: SEA 6111
(Copy Nos.16 and 17)

Commander
Naval Sea Systems Command
Department of the Navy
Washington, D.C. 20362
Attn: SEA 6113
(Copy Nos.18 and 19)

Commander
Naval Sea Systems Command
Department of the Navy
Washington, D.C. 20362
Attn: SEA 6120
(Copy Nos. 20 and 21)

Commander
Naval Sea Systems Command
Department of the Navy
Washington, D.C. 20362
Attn: SEA 3232
(Copy No. 22)

Officer in Charge
David W. Taylor Naval Ship
Research and Development Center
Annapolis Laboratory
Annapolis, MD 21402
Attn: Mr. J. Smith
(Copy No. 23)

Officer in Charge
David W. Taylor Naval Ship
Research and Development Center
Annapolis Laboratory
Annapolis, MD 21402
Attn: Mr. L. J. Argiro
(Copy Nos. 24, 25, 26, 26, 28, 29)

Commander
David W. Taylor Naval Ship Research
and Development Center
Bethesda, MD 20084
Attn: Dr. M. Sevik
(Copy Nos. 30 and 31)

Commander
David W. Taylor Naval Ship Research
and Development Center
Bethesda, MD 20084
Attn: Dr. W. W. Murray
(Copy Nos. 32 and 33)

Commander
David W. Taylor Naval Ship Research
and Development Center
Bethesda, MD 20084
Attn: Dr. M. Strasberg
(Copy No. 34)

Commander
David W. Taylor Naval Ship Research
and Development Center
Bethesda, MD 20084
Attn: Dr. G. Maidanik
(Copy No. 35)

Commander
David W. Taylor Naval Ship Research
and Development Center
Bethesda, MD 20084
Attn: Dr. G. Chertock
(Copy No. 36)

Commander
David W. Taylor Naval Ship Research
and Development Center
Bethesda, MD 20084
Attn: Dr. D. Feit
(Copy Nos. 37,38,39,40, 41, 42)

Commander
David W. Taylor Naval Ship Research
and Development Center
Bethesda, MD 20084
Attn: Mr. J. T. Shen
(Copy No. 43)

Director
Defense Documentation Center
Cameron Station
Alexandria, VA 22314
(Copy Nos. 44, 45, 46, 47, 48, 49,
50, 51, 52, 53, 54, 55)

Director
Naval Research Laboratory
Washington, D.C. 20390
Attn. Code 8440
(Copy Nos. 56 and 57)

Ocean Structures Branch
U.S. Naval Research Laboratory
Washington, D.C. 20390
Attn: Mr. G. J. O'Hara
(Copy No. 58)

Office of Naval Research
Department of the Navy
Arlington, VA 22217
Attn: Dr. G. Boyer
(Copy No. 59, 60, 61)

Office of Naval Research
Department of the Navy
Arlington, VA 22217
Attn: Dr. A. O. Sykes
(Copy Nos. 62, 63, 64)

Office of Naval Research
Department of the Navy
Arlington, VA 22217
Attn: Mr. Keith M. Ellingsworth
(Copy No. 65)

Office of Naval Research
Department of the Navy
Arlington, VA 22217
Attn: Dr. N. Perrone
(Copy NO. 66)

Commander
Mare Island Naval Shipyard
Vallejo, CA 94592
(Design Division)
(Copy No. 67)

Commander
Portsmouth Naval Shipyard
Portsmouth, NH 03801
(Copy No. 68)

Supervisor of Shipbuilding,
Conversion and Repair
General Dynamics Corporation
Electric Boat Division
Groton, CT 06340
Attn: Mr. John Wilder
Dept. 440
(Copy Nos. 69 and 70)

Supervisor of Shipbuilding,
Conversion and Repair
Ingalls Shipbuilding Corporation
Pascagoula, MS 39567
(Copy No. 71)

Supervisor of Shipbuilding,
Conversion and Repair
Newport News Shipbuilding
Newport News, VA 23607
(Copy No. 72)

Naval Ship Research and Development
Center
Underwater Explosion Research
Division
Portsmouth, VA 23709
(Copy No. 73)

Commander
Naval Underwater Systems Center
New London Laboratory
New London, CT 06320
Attn: Mr. G. F. Carey
(Copy No. 74)

Commander
Naval Underwater Systems Center
New London Laboratory
New London, CT 06320
Attn: Dr. R. S. Woollett
(Copy No. 75)

Commander
Naval Ocean Systems Center
San Diego, CA 92052
Attn: Library
(Copy No. 76)

Dr. J. Barger
Bolt Beranek and Newman, Inc.
50 Moulton Street
Cambridge, MA 02138
(Copy No. 77)

Dr. D. I. G. Jones
Air Force Materials Laboratory
Wright-Patterson Air Force Base
Ohio 45433
(Copy No. 78)

Dr. M. C. Junger, President
Cambridge Acoustical Associates, Inc.
54 Rindge Avenue
Cambridge, MA 02140
(Copy No. 79)

Acquisitions Supervisor
Technical Information Service
American Institute of Aeronautics
and Astronautics, Inc.
750 Third Avenue
New York, NY 10017
(Copy No. 80)

Dr. R. S. Ayre
Department of Civil Engineering
University of Colorado
Boulder, CO 80302
(Copy No. 81)

Dr. D. Frederick
Chairman, Engineering Science and
Mechanics Department
Virginia Polytechnic Institute
and State University
Blacksburg, VA 24061
(Copy No. 82)

Dr. D. E. Hudson
Department of Mechanics
California Institute of Technology
Pasadena, CA 91109
(Copy No. 83)

Dr. G. Herrman, Chairman
Department of Applied Mechanics
Stanford University
Stanford, CA 94305
(Copy No. 84)

Dr. A. Kalnins
Department of Mechanical Engineering
and Mechanics
Lehigh University
Bethlehem, PA 18015
(Copy No. 85)

Dr. Y. H. Pao, Chairman
Department of Theoretical and
Applied Mechanics
Cornell University
Ithaca, NY 14850
(Copy No. 86)

Dr. D. D. Kana
Southwest Research Institute
8500 Culebra Road
San Antonio, TX 78206
(Copy No. 87)

Dr. J. R. Rice
School of Engineering
Brown University
Providence, RI 02912
(Copy No. 88)

Dr. P. S. Symonds
School of Engineering
Brown University
Providence, RI 02912
(Copy No. 89)

Dr. W. J. Worley
Department of Theoretical and
Applied Mechanics
University of Illinois
Urbana, IL 61801
(Copy No. 90)

Dr. Dana Young
Southwest Research Institute
8500 Culebra Road
San Antonio, TX 78206
(Copy No. 91)

Dr. R. M. Gorman
Bolt Beranek and Newman, Inc.
Union Station
New London, CT 06340
(Copy No. 92)

Commander
Naval Sea Systems Command
Department of the Navy
Washington, D.C. 20362
Attn: SEA 9661-Library
(Copy No. 93 and 94)